Network representation in hydrological modelling on urban catchments in data-scarce contexts: A case study on the Oued Fez catchment (Morocco)

Ismail Bouizrou, Nanée Chahinian, Jean-Louis Perrin, Rémi Müller, Naoual Rais

Journal of Hydrology: Regional Studies 34 (2021) 100800

Contents lists available at ScienceDirect

Journal of Hydrology: Regional Studies

journal homepage: www.elsevier.com/locate/ejrh

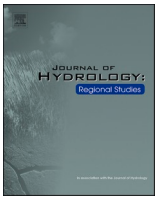

Network representation in hydrological modelling on urban catchments in data-scarce contexts: A case study on the Oued Fez catchment (Morocco)

Ismail Bouizrou [a], Nanée Chahinian [b,*], Jean-Louis Perrin [b], Rémi Müller [b], Naoual Rais [a]

[a] *Functional Ecology and Environmental Engineering Laboratory, Sidi Mohamed Ben Abdellah University, Faculty of Sciences and Techniques, Morocco*
[b] *HSM, Univ Montpellier, CNRS, IRD, France*

ARTICLE INFO

Keywords:
Hydrological modelling
Flood events
Urbanisation
Distributed hydrological models
ATHYS
Oued Fez catchment

ABSTRACT

Study region: Oued Fez, Morocco.
Study focus: Urban catchments are heterogeneous in terms of land use and have both natural and artificial drainage networks. Modelling them is not a straightforward task especially in data-scarce settings. This study investigates network representation in hydrological modelling using field data collected between 2008 and 2018 on the Oued Fez catchment. The road network is used as a proxy for the stormwater network. Two production functions, SCS (1972) and a linear reservoir, are coupled to the lag and route transfer function. Three types of land use classes are used. Tests are carried out at hourly and 5-minute time steps using both the natural and modified drainage networks.
New hydrological insights for the region: Fifty-three rainfall–runoff events are monitored on the urban part of the catchment over the 2008–2018 period. The highest rainfall values are recorded in 2008/2009, while the highest peak flow values are recorded in 2017/2018. This is due to stream channelisation and increased stormwater network coverage. Using the road network with minimal land use classes improves the model performance at both the hourly and 5-minute time steps.

1. Introduction

The complexity of urban catchments is a challenge for hydrological studies due to the presence of artificial drainage networks and the high spatial variability of the urban fabric. In order to model such catchments, these particularities need to be considered. A significant number of studies have been carried out on urbanisation and its influence on the hydrological behaviour of urban catchments. Urban sprawl leads to fundamental disturbances in hydrological systems (Güneralp et al., 2015; Zambrano et al., 2018). Salvadore et al. (2015) have indicated that drainage directions are often artificially modified on urban catchments, and that this increases consequently the magnitude and frequency of floods. Urbanisation is also known to increase flow velocity, runoff volume and

* Corresponding author at: UMR HydroSciences Montpellier, Université Montpellier CC 57, 163 rue Auguste Broussonnet, 34090, Montpellier, France.
E-mail address: nanee.chahinian@ird.fr (N. Chahinian).

https://doi.org/10.1016/j.ejrh.2021.100800
Received 16 May 2020; Received in revised form 19 November 2020; Accepted 25 February 2021
Available online 5 March 2021

reduce infiltration rates (Huang et al., 2008; Du et al., 2012; Fletcher et al., 2013; Miller et al., 2014; Xu and Zhao, 2016; Habibi and Seo, 2018). Other studies have focused on the impact of impervious surfaces on runoff generation. Palla and Gnecco (2015) stated that land artificialisation through increased impervious surfaces promotes surface runoff, Segond et al. (2007) have shown that on impervious areas, a high proportion of rainfall becomes effective and produces runoff, contrary to pervious areas. In addition, the time to peak of the flood hydrographs decreases and peak flow increases (Huang et al., 2008).

Accounting for the spatial heterogeneity of urban catchments in hydrological modelling requires the use of high-resolution data and complex spatially distributed hydrological models (Salvadore et al., 2015; Fatichi et al., 2016). However, complexity in the models does not guarantee a better performance (Pérez-Sánchez et al., 2019), since complex models involve more parameters that may translate into a large number of parameters to be calibrated. When limited observational data is available, a high risk of over-parameterisation may occur (Andréassian et al., 2012). The challenge hence is to find this equilibrium.

Since the 1970s, many models have been developed to study the hydrological behaviour of urban catchments or to manage them (Zoppou, 2000; Rodriguez et al., 2003; Bach et al., 2014; Salvadore et al., 2015; Cristiano et al., 2018). SWMM (Huber and Dickinson, 1988) is one of the most documented ones and has been used in a number of studies (Barco et al., 2008; Krebs et al., 2014; Leandro and Martins, 2016; Yao et al., 2016). Hydraulic models such as CANOE (INSAVALOR, SOGREAH, 1997) and MIKE (Refsgaard and Storm, 1995) have also been used to model runoff (Lhomme et al., 2004; Hamouda and Lahbassi, 2012). These models' spatial discretisation schemes account for the layout of the stormwater network. Most of these models represent the inlets and manholes as nodes and the conduits as segments (Schmitt et al., 2004; Rodriguez et al., 2003 and 2008; Chen et al., 2018). The difference lies in the representation of the surface flow units. Some use triangular networks to discretise the streets (Schmitt et al., 2004), crossroads (Paquier et al., 2015) and buildings (Fewtrell et al., 2008; Leandro et al., 2016). Others use a semi-distributed approach for surface flow including hydrological units, cadastral parcels, river elements and streets (Rodriguez et al., 2003 and 2008; Jankowfsky et al., 2014; Chen et al., 2018).

However, the data needed to run these models is not always available: in some developing and developed countries, accurate maps of the stormwater and wastewater networks are not available (Chahinian et al., 2019). Hence, some authors have also tried to adapt "generic" hydrological models to urban catchments (Perrin and Bouvier, 2004; Lhomme et al., 2006; Bouvier et al., 2018; Aliyari et al., 2019). These approaches are thought to be well adapted to large-scale catchments and metropolitan areas, especially in data-scarce regions.

An important feature of distributed hydrological models is the drainage network, and that of urban catchments has been the object of particular interest in the literature. It is now established that urbanisation decreases dramatically the natural channel density (Graf, 1977; Meyer and Wallace, 2001). Indeed, in an attempt to control flows and allow urban development, natural channels are often buried or covered and as such are no longer visible to the naked eye or reported on maps. Thus, simply using drainage network extraction procedures based on Digital Terrain Models (O'Callaghan and Mark, 1984; Tarboton et al., 1991) might not be sufficient.

In addition, urbanisation also leads to the development of artificial drainage networks, which increase the overall drainage density (Graf, 1977) by adding artificial links. Roads in particular are reported to increase drainage by providing new trajectories for surface water (Bannister, 1979), concentrating flows and increasing their velocity (Shuster et al., 2005). According to Ogden et al. (2011), the increases in drainage density, particularly when moving from low values to middle and high values, produce significant increases in the flood peaks. However, drainage density is reported to have an asymptotic behaviour and, beyond a threshold value, its influence is less on peak flow and runoff volume (Ogden et al., 2011). Kroczak and Bryndal (2015) have shown that the incorporation of the road

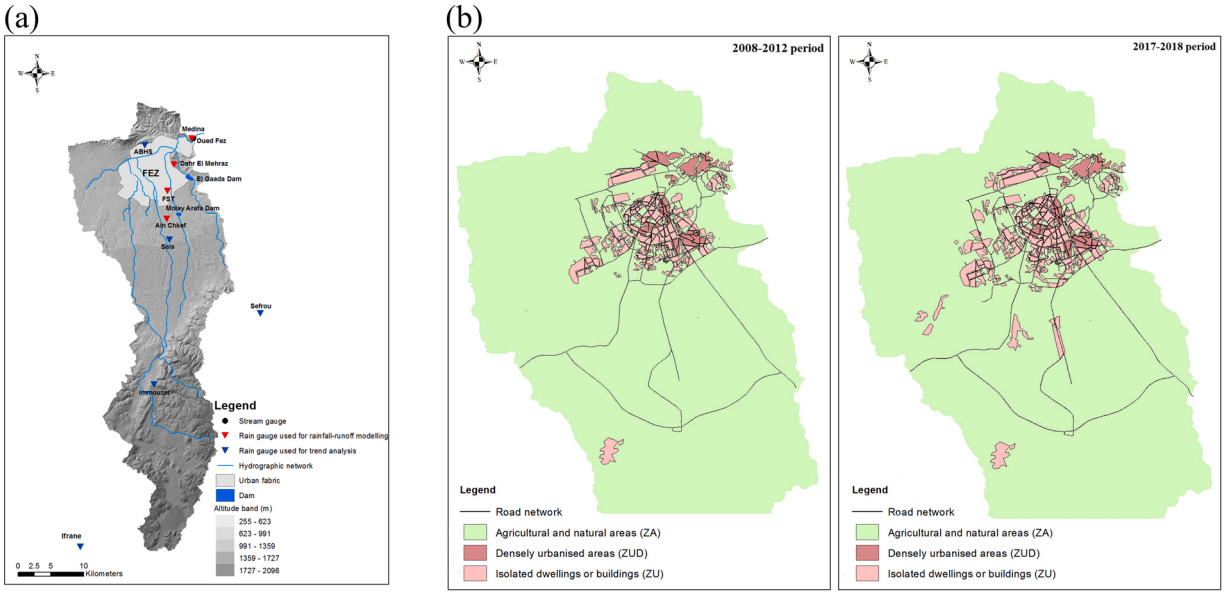

Fig. 1. The Oued Fez catchment: a) study area; b) the land use classes of urban part.

network improves flood simulation significantly. These authors conclude that the spatial distribution of impervious surfaces has a marked effect on the hydrological response, and emphasise the need to use a distributed model, which allows the incorporation of detailed rainfall information as well as the imperviousness of the study zone.

Oued Fez is a perfect example of these urban catchments, where the extent of urbanisation strongly impacts the hydrological response. A number of studies (Lombard-Latune et al., 2010; Reynard et al., 2013; Akdim et al., 2013) highlighted the particularity of the study area, characterised by high spatial variability of rainfall and strong spatial heterogeneity of land use, namely in the downstream part which is highly urbanised. A first modelling attempt was carried out by Lombard-Latune et al. (2010) using a lumped model. Thus, the representation and impact of the catchment's drainage network could not be assessed. The objective of the work is to investigate network representation in hydrological modelling on urban catchments in data-scarce contexts by using a distributed approach using a generic distributed hydrological model and the road network as a proxy for urban water networks. Tests are carried out using the natural drainage network and a modified drainage network that includes the road network. With this aim, two production functions and two parameterisation schemes are compared at hourly and five-minute time steps. After a brief description of the study area's characteristics and available data, a detailed overview of the tested hydrological models will be given. Finally, the main results will be presented, analysed and discussed.

2. Materials and methods

2.1. The Oued Fez catchment

Oued Fez (Fig. 1a) is a tributary of the Sebou, which is the largest river system in Morocco. Covering a total area of 814 km^2, this

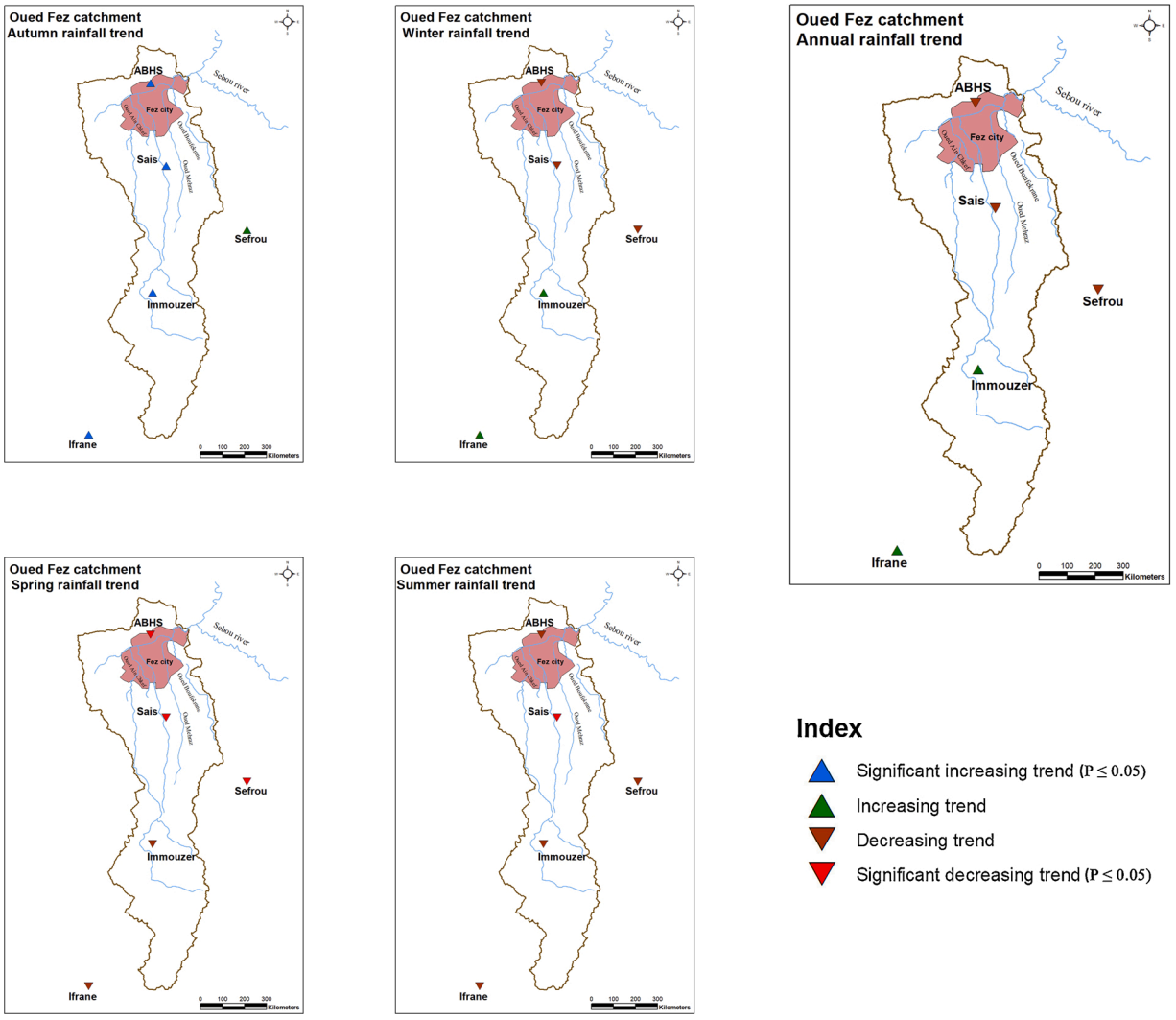

Fig. 2. Mann–Kendall trend test result for rainfall at annual and seasonal scales (1972–2015).

catchment is drained by a dense hydrographical network and has Oued Fez as its main tributary.

Oued Fez flows in an easterly direction from the karstic spring of Ras El Ma through the city of Fez. Its main tributaries, Oueds Boufekrane, El Mehraz and Ain Chkef, pour into Oued Fez in the urban area and the river then flows into the Sebou, 4 km downstream of the city. The catchment is considered urban since more than 10 % of its area is located within the city of Fez, where the medina (old city) is heavily built-up and represents the craft centre of the city (Lombard-Latune et al., 2010).

The catchment can be divided into two parts based on the predominant land use types: natural karstic zones in the upstream part and urban in the downstream part. In order to reduce flooding, two dams have been constructed on the Oued Fez catchment. The Molay Arafa Dam was built on Oued El Mehraz in 1993 with a capacity of 0.60 Mm^3, the El Gaada Dam was built on Oued Boufekrane in 1991 with a capacity of 2.90 Mm^3. In addition, a diversion channel, with an evacuation capacity of 35 $m^3.s^{-1}$, was built to divert part of the water stored in the Molay Arafa Dam to the El Gaada Dam (METLE, 2020).

The catchment is located on two groundwater systems, a deep Triassic aquifer and the shallow unconfined Sais aquifer. Falling piezometric levels due to a combination of over-exploitation and droughts have been reported for both since the end of the 1970s (ABHS, 2005). The pedologic cover of the catchment is dominated by calcimagnesic soils and to a lesser extent by vertisols, then by scattered alluvial soils (Bellarbi et al., 2011).

The prevailing climate is semi-arid continental characterised by hot dry summers and cold wet winters. In the absence of mean daily temperatures, we used the mean monthly temperatures to estimate the mean annual temperature, whose value is 16.9 °C for the 1970–2011 period at the Fez-Sais station. For the same period, the mean annual potential evapotranspiration (PET) is 863 mm.$year^{-1}$ using Thornthwaite's method. This method was chosen because it relies only on temperature data.

Time series of annual and monthly rainfall from 1972 to 2015 (44 years) collected by the Sebou River Basin Authority (Agence du Bassin Hydraulique de Sebou-ABHS) have been used to analyse annual and seasonal trends in rainfall. Five rain gauges for which long records are available are used for the study, three of which are located on the Oued Fez catchment. The remaining two are within the Sebou catchment boundaries but outside our study area (Fig. 1a). The Mann–Kendall test (Mann, 1945; Kendall, 1975), which is widely used to detect trends in time series of meteorological variables (see a review in Yue et al., 2002 and Kisi, 2015) and is well adapted to study rainfall variation (Hamed, 2008; Tabari and Talaee, 2011; Jain and Kumar, 2012), is used. It is combined with Sen's slope test (Sen, 1968) to detect the magnitude of these trends.

The trend analysis has been carried out on all rain gauges at seasonal and yearly time steps. Since the lag-1 correlation showed no significant serial correlation, the Mann–Kendall test was used directly without the need for a pre-whitening procedure. The results (Fig. 2) show that at the annual timescale, the Ifrane and Immouzzer rain gauges which are located in the upstream part of the study area have a positive but statistically non-significant trend at a significance level α of 5% ($p \leq 0.05$). Going downstream, a negative but statistically non-significant trend ($p \leq 0.05$) can be observed for the Sefrou, Sais and ABHS stations. Similar trends were also identified for the winter season. For all the rain gauges in the study area, spring and summer have negative trends, while autumn show a positive trend.

The magnitude of rainfall trends has also been characterised using Sen's Slope test (Table 1). An increase in annual rainfall at a rate of 0.40 mm.$year^{-1}$ is detected over the study period: the rainy seasons (autumn and winter) are characterised by an increase in rainfall rates (2.71 and 0.25 mm.$year^{-1}$ respectively), while a decrease in rainfall rates with values of -0.12 and -1.97 mm.$year^{-1}$ is observed for the summer and spring seasons. The Precipitation Concentration Index (PCI, Oliver, 1980) is used to study the concentration of annual precipitation and its spatial variation over the entire study area (De Luis et al., 2011; Amiri and Mesgari, 2017). It is calculated at an annual timescale using the following equation:

$$PCI\text{annual} = \frac{\sum_{i=1}^{12} Pi2}{\left(\sum_{i=1}^{12} Pi\right)2} \cdot 100 \quad (1)$$

Where p_i refers to the monthly precipitation for month i [L].

According to Olivier (1980), PCI values < 10 indicate a low precipitation concentration, i.e. uniform precipitation, while PCI > 20 shows very high concentration and strong irregularity.

The results (Table 2) show that the Oued Fez catchment is characterised by an irregular distribution of precipitation with mean values of PCI ranging from 16 to 19. The irregularity of the rainfall distribution increases when moving downstream: the ABHS and Sais rain gauges located in the city of Fez (downstream part) have higher values of PCI (19 and 18 respectively), while the rain gauges located in the upstream zone (Immouzzer, Sefrou and Ifrane rain gauges) have PCI values of around 16. This increased irregularity of rainfall may be partly explained by the gradual increase in urbanisation: urban development is lower in the upstream part of the

Table 1
Coefficient of Variation and Sen's slope values for seasonal and annual rainfall.

Time step	Sen's slope	Coefficient of Variation (%)
Spring	−1.97	37
Summer	−0.12	70
Autumn	2.71	47
Winter	0.26	47
Annual	0.4	25

catchment and higher in the downstream part where the city of Fez is located. This is known to have an impact on atmospheric dynamics at a local scale and to affect rainfall distribution (Salvadore et al., 2015). Consequently, storms can be highly localised (Maier et al., 2020).

Although there is no clear consensus on this issue, most studies emphasise that urbanisation has an important impact on rainfall in terms of rainfall intensity and its spatial distribution. For instance, Zhu et al. (2019) and Zhang et al. (2007) concluded that urbanisation can potentially increase the precipitation intensity in mega-cities such as Beijing. The effects of urbanisation on summertime precipitation were also assessed in Osaka, Japan by Shimadera et al. (2015), who showed that urbanisation increased not only the precipitation intensity but also its duration. Furthermore, Liang and Ding (2017) studied the effect of urbanisation on the long-term variation of extreme precipitation over Shanghai and showed that urbanisation increased the frequency and intensity of rainfall. However, the effect of urbanisation on the total amount of rainfall was found to be different and no conclusion could be drawn. Indeed, while some authors found that urbanisation increased total rainfall (Shimadera et al., 2015; Liang and Ding, 2017; Zhu et al., 2019), others concluded that urbanisation decreased total rainfall (Guo et al., 2006; Zhang et al., 2007). The different trends of total rainfall in urban areas could be attributed partly to the difficulty in separating atmospheric circulation and local topographic effects, as most cities are located in different geographic and climatic conditions, have different regional circulation and possibly have different urban aerosol emissions (Guo et al., 2006).

2.2. The experimental setting in the urban and peri-urban sub-catchment of Oued Fez

The urban and peri-urban sub-catchment of Oued Fez covers an area of 397 km^2 (Fig. 1b). Since 2008, our team has collected discharge and rainfall data in this zone. In September 2008, a stream gauge was installed at the catchment outlet. The water level is automatically recorded every five minutes by means of a pressure transducer (PDCR 1830, 700 mbar, Druck) and subsequently converted into discharge using a rating curve established by our research team. Over the 2008–2017 period, three rating curves were established. The first one was valid from 01/10/2008 to 30/11/2010, the second one from 30/11/2010 to 01/01/2014 and the last one has been valid since 01/01/2017. Eight stream flow gauging campaigns were used to establish the first two rating curves, which were obtained by fitting a second-degree polynomial. Four campaigns were used to establish the third rating curve. A full topographical survey was carried out as the river bed had been modified following works by the water agency. Note that at 0.90 m the gauging station is flooded. The third rating curve was established using the BaRatin method (Le Coz et al., 2013), which has the advantage of taking into account the hydraulic controls of the cross-section and producing uncertainty estimates due to the stage graphs and the parameters of the function used to fit the rating curve. The last measured stage value for the current rating curve is 0.57 m, corresponding to a discharge value of 0.57 $m^3.s^{-1}$ when disregarding all sources of errors. The last extrapolated stage value is 0.71 m, corresponding to a discharge value of 2.87 $m^3.s^{-1}$.

A monitoring network composed of four rain gauges has been gradually implemented in the urban part of Oued Fez. Rainfall is measured by means of tipping bucket (0.20 mm) rain gauges. Note that for the 2008–2009 period rainfall was recorded at 12-minute intervals by FST Fez's physics department. For the rain gauges implemented later, rainfall was measured at 5-minute intervals. Fig. 3 shows hourly streamflow series from 2008 to 2018. An important variability of streamflow especially in terms of peak flows can be observed. Note that no flows were recorded between January and April 2010, as our gauging station was flooded. The water agency also undertook works in the river bed and the discharge measurements were suspended between 2014 and 2016. Higher mean flows were recorded during the 2008/2009 period, which was exceptionally wet and characterised by a high number of rainy days.

In terms of peak flow, the 2017/2018 period has the highest values, 2008/2009 can be considered as an intermediate period, while 2011/2012 has the lowest values of peak flow. The high values observed for the 2017/2018 period can be explained mainly by the fact that, since 2014, several portions of the Oued Fez, El Mehraz and Ain Chkef rivers have been canalised.

Flow conditions have also been impacted by the implementation of a new wastewater treatment plant in Fez in 2014. The station has a treatment capacity of 1.2 M EQH and a daily discharge of 155400 m^3. Up to its construction, all of the city's sewage was flushed directly into the river (Koukkal et al., 2004; Perrin et al., 2014). The temporal dynamics of the effluent discharge was assessed by gauging a sewage canal located to the right of the gauging station located on Oued Fez. This canal was originally built as part of a wastewater pre-treatment facility and was used to convey water to a small hydro-electric plant. Nowadays it flows into the Fez wastewater treatment plant but may overflow occasionally. The results of our gauging campaign on September 15th 2010, an ordinary working day, showed that wastewater discharge in the canal increased from 1.06 $m^3.s^{-1}$ at 07:45 A.M. to 1.76 $m^3.s^{-1}$ at 10:13 A.M., reached a maximum value of 1.95 $m^3.s^{-1}$ at 2:40 P.M., and remained at 18.40 $m^3.s^{-1}$ at 4:40 P.M. Note that wastewater dynamics may vary during the Ramadan period when water and food consumption is prohibited until fast-breaking time, and at the height of the touristic season. The temporal dynamics may also be assessed using Oued Fez's discharge time series on rainless days using a baseflow separation method (Eckhardt, 2008; Stewart, 2015). However, in order to quantify it accurately, the discharge of the springs that flow into Oued Fez should be subtracted and we do not have this information.

Table 2
Precipitation Concentration Index values.

Index	PCI Value				
	ABHS	Ifrane	Immouzzer	Sais	Sefrou
PCI	19	17	16	18	16

A PCI > 16 indicates irregular precipitation.

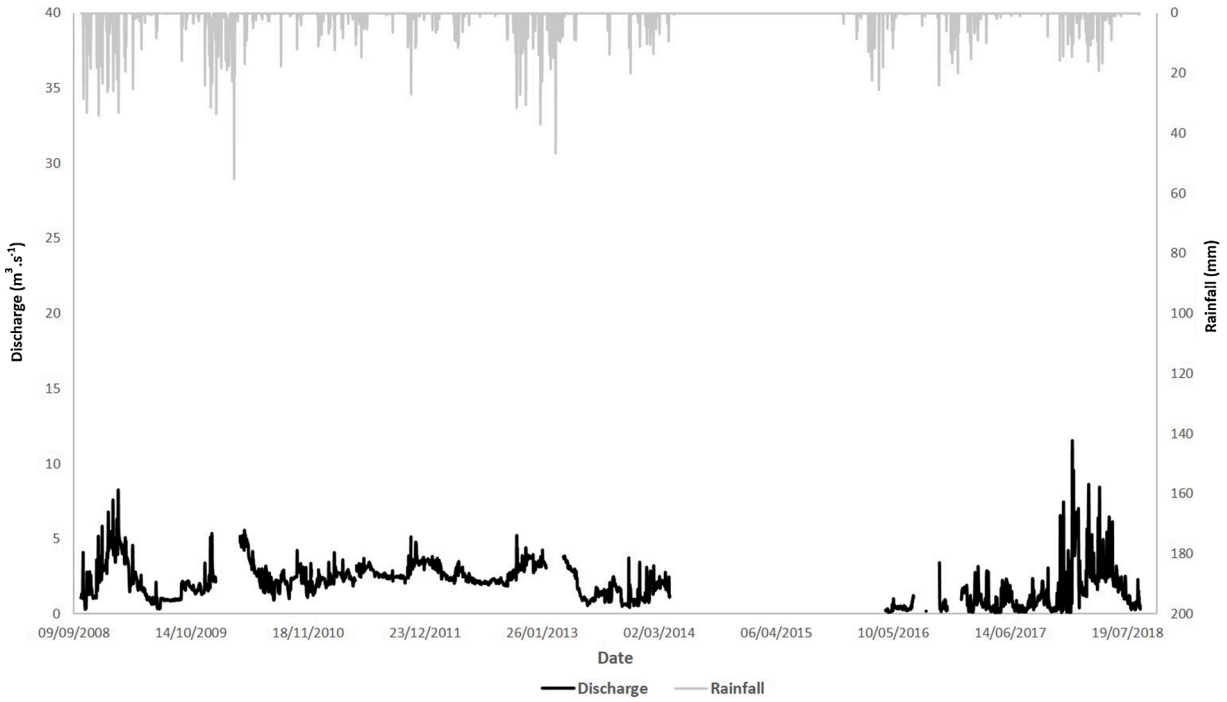

Fig. 3. Rainfall and discharge values recorded in the urban sub-catchment of Oued Fez over the study period.

Before 2009 the wastewater network consisted mainly of combined sewers with a total length of 2050 km. The circular pipes had diameters ranging between 300 and 1600 mm while the ovoids had heights ranging between T100 and T240 (Amarti Riffi, 2013). Between 2010 and 2016, the stormwater coverage improved and is now over 99 % (MUAT, 2016). Currently stormwater overflows occur only when the wastewater treatment plant is out of service. Despite our best efforts, we could not get quantifiable data on the updated network, namely a map detailing its layout and attributes. Hence, we could not use a hydraulic model to specifically model the water flow in the pipes and sewer overflows. We had to resort to a simpler modelling approach and use the street network as a proxy for the stormwater network. Our hypothesis is that, as per design rules, both networks are laid either under the pavement or the road. Thus, we could indirectly account for the flow dynamics and different travel times.

Our study focuses on rainfall–runoff events. Not all four rainfall gauges were operational over the study period. This was due to the gradual deployment of the monitoring network and to equipment breakdown. Thereby a strict quality control procedure was conducted by considering the breakdown periods and removing outlier values. We retained a threshold of 6 mm for rainfall events and a time gap of 30 min to separate two consecutive events. Through this operation, 53 flood events corresponding to three periods were chosen for rainfall–runoff modelling (Table 3).

- The 2008–2009 period: This period includes 17 flood events. Rainfall varies between 6 and 40.2 mm, maximum rainfall intensity at an hourly time step ranges from 3.24 to 13.1 $mm.h^{-1}$ (45.6–144 $mm.h^{-1}$for dt = 12 min) and discharge from 1.5 to 44 $m^3.s^{-1}$.
- The 2011–2012 period: This period includes 16 flood events. Total rainfall varies between 8.2 mm and 31.3 mm, maximum rainfall intensity at an hourly time step varies between 2.5 and 10.2 $mm.h^{-1}$ (4.5 and 56.4 $mm.h^{-1}$ for dt = 5 min) and discharge from 3.5 to 8 $m^3.s^{-1}$.
- The 2017–2018 period: 20 flood events were recorded during the third period using all four rainfall gauges. Total rainfall varies between 7.0 and 29.6 mm, maximum rainfall intensity at an hourly step varies between 2.3 and 7.6 $mm.h^{-1}$ (5.7 and 36.6 $mm.h^{-1}$ for dt = 5 min) and discharge between 7.9 and 38.7 $m^3.s^{-1}$.

Of the events in our sample, 1% occurred in the summer. The most important flood events in terms of runoff depth and peak flow are recorded in winter. To investigate the catchment's hydrological behaviour and signature, we investigated the rainfall–runoff relationship (McMillan et al., 2017; Addor et al., 2018). Hydrological signatures may be calculated based on a variety of data sources, but in practice, they are usually based on discharge time series (Addor et al., 2018). Since we only have streamflow measurements and simulations at the catchment outlet, we have carried out a comparison on the rainfall–runoff relationships between 2008–2012 and 2017–2018 in order to determine the hydrological similarity or changes across the two periods. The results presented in Fig. 4 show a linear relationship, with a good correlation between rainfall and observed runoff for the flood events of the 2008–2012 period (R^2 = 0.74). By contrast, there is no linear relationship or correlation between rainfall and observed runoff for the flood events belonging to the 2017–2018 period (R^2 = 0.17). This change may be due to the increasing imperviousness caused by urban development, channelisation of watercourses and the extension of drainage networks (Guan et al., 2016; Wang et al., 2020), which leads to a flash runoff

Table 3
Main characteristics of the rainfall–runoff events recorded during the 2012–2018 period.

Event number	Event date	Calibration (C) or validation (V)	Number of rain gauges	Duration (min)	Rainfall (mm)	Maximum rainfall intensity (mm. h^{-1}) dt =60 min	Qp_{Obs} ($m^3.s^{-1}$)
1	10/10/2008	C	1	840	26.80	13.20	13.06
2	22/10/2008	V	1	1140	24.00	6.20	11.25
3	28/10/2008	C	1	660	10.00	3.00	3.82
4	01/11/2008	V	1	1380	20.20	3.40	4.55
5	25/11/2008	C	1	1260	33.40	6.20	7.17
6	29/11/2008	V	1	840	10.20	2.40	3.24
7	30/11/2008	V	1	780	16.20	6.00	10.32
8	01/12/2008	V	1	1740	33.30	6.00	9.36
9	09/12/2008	C	1	1320	17.60	4.00	8.84
10	12/12/2008	V	1	600	7.60	3.00	5.98
11	14/12/2008	C	1	1620	34.00	6.80	10.68
12	28/12/2008	C	1	600	6.00	2.60	4.07
13	31/12/2008	V	1	1260	26.00	2.80	5.53
14	02/01/2009	C	1	660	8.80	2.80	3.70
15	20/01/2009	C	1	1140	34.00	6.20	10.16
16	06/02/2009	V	1	1140	15.40	2.20	4.03
17	07/02/2009	C	1	1620	40.20	5.40	10.28
18	29/04/2011	C	1	1310	29.80	5.50	9.51
19	01/05/2011	V	1	835	14.80	8.40	8.61
20	27/05/2011	C	1	2060	11.40	9.80	7.08
21	24/10/2011	C	2	815	15.20	5.70	6.08
22	04/11/2011	V	2	925	20.30	3.25	4.70
23	04/11/2011	V	2	765	28.25	6.20	6.98
24	19/11/2011	V	2	1055	13.30	2.80	4.45
25	01/04/2012	C	2	710	13.20	8.50	6.14
26	29/10/2012	C	4	1300	28.08	4.70	4.75
27	30/10/2012	V	4	1250	30.48	6.43	6.72
28	31/10/2012	C	4	1360	26.05	6.55	5.83
29	11/11/2012	C	4	1380	31.35	10.20	7.21
30	18/11/2012	V	4	950	13.80	3.28	3.10
31	30/11/2012	C	4	1050	14.13	3.68	4.38
32	07/12/2012	V	4	1310	8.15	2.48	2.34
33	25/12/2012	V	4	820	11.63	7.58	5.51

(*continued on next page*)

Table 3 (*continued*)

Event number	Event date	Calibration (C) or validation (V)	Number of rain gauges	Duration (min)	Rainfall (mm)	Maximum rainfall intensity (mm. h^{-1}) dt =60 min	Qp_{Obs} ($m^3.s^{-1}$)
34	27/01/2017	C	4	435	9.63	3.00	4.40
35	22/02/2017	C	4	655	8.68	5.88	23.29
36	23/02/2017	C	4	2290	6.95	2.25	5.91
37	12/05/2017	V	4	410	7.65	3.38	10.16
38	29/11/2017	C	4	275	6.98	5.40	15.13
39	11/12/2017	C	4	745	21.28	6.88	20.85
40	27/12/2017	V	4	795	16.25	4.63	30.73
41	06/01/2018	V	4	1085	11.70	2.73	12.70
42	08/01/2018	V	4	520	12.30	6.98	26.95
43	09/01/2018	C	4	1650	29.63	4.70	32.07
44	04/02/2018	V	4	1540	16.68	5.78	17.28
45	26/02/2018	V	4	940	12.38	4.28	9.83
46	28/02/2018	V	4	2140	24.75	5.88	19.56
47	03/03/2018	C	4	420	7.63	3.33	10.14
48	05/03/2018	C	4	510	8.78	7.60	15.64
49	06/03/2018	V	4	500	21.00	5.70	21.10
50	24/03/2018	V	4	1000	7.93	3.55	9.41
51	09/04/2018	C	4	705	8.33	2.75	9.73
52	10/04/2018	V	4	1035	12.28	6.30	20.53
53	12/04/2018	V	4	1025	17.05	6.06	16.88

response to rainstorms (Burns et al., 2005) and an increase of total runoff (Wang et al., 2020), namely during uniform, low intensity rainfall events (Guan et al., 2016). For instance, the events of 22/10/2008 and 12/04/2018, both occurring in wet conditions, had maximum rainfall intensities of 6.20 and 6 $mm.h^{-1}$, respectively, and produced 534 mm and 914 mm of runoff for total rainfall values and durations of the same order of magnitude. The decrease of R^2 could have been caused by greater uncertainty on higher runoff values due to measurement errors and the extrapolation of the rating curve. However, we do not think that is the case in this study since the highest rainfall, runoff and peak flow values, all events considered, were recorded during the 2008–2009 period.

2.3. The models

The ATHYS modelling platform (http://www.athys-soft.org; Bouvier and Delclaux, 1996) was chosen for this work. It is a spatially distributed hydrological modelling platform which includes several production functions that assimilate the soil to a linear reservoir. The reservoir is fed through infiltrated rain and the drainage losses represent both evaporation and percolation. A portion of the drainage losses may contribute to sub-surface flow (Fig. 5a).

A literature review of the available models in the ATHYS platform was carried out in order to identify the ones most adapted to the urban and semi-arid nature of the catchment. Another important consideration was the data available on the study zone: since we did not have access to data on the soils' hydrodynamic properties, we had to resort to empirical models. In addition, given the fact that runoff is mainly due to Hortonian overland flow on this catchment, we could not use TOMODEL (Beven and Kirkby, 1979; Franchini et al., 1996; Beven, 1997), which assumes saturation excess flow. As a result, two production functions, SCS and a variable runoff coefficient function, were selected and combined with the lag & route transfer function. Their main work hypotheses are detailed in the sections below.

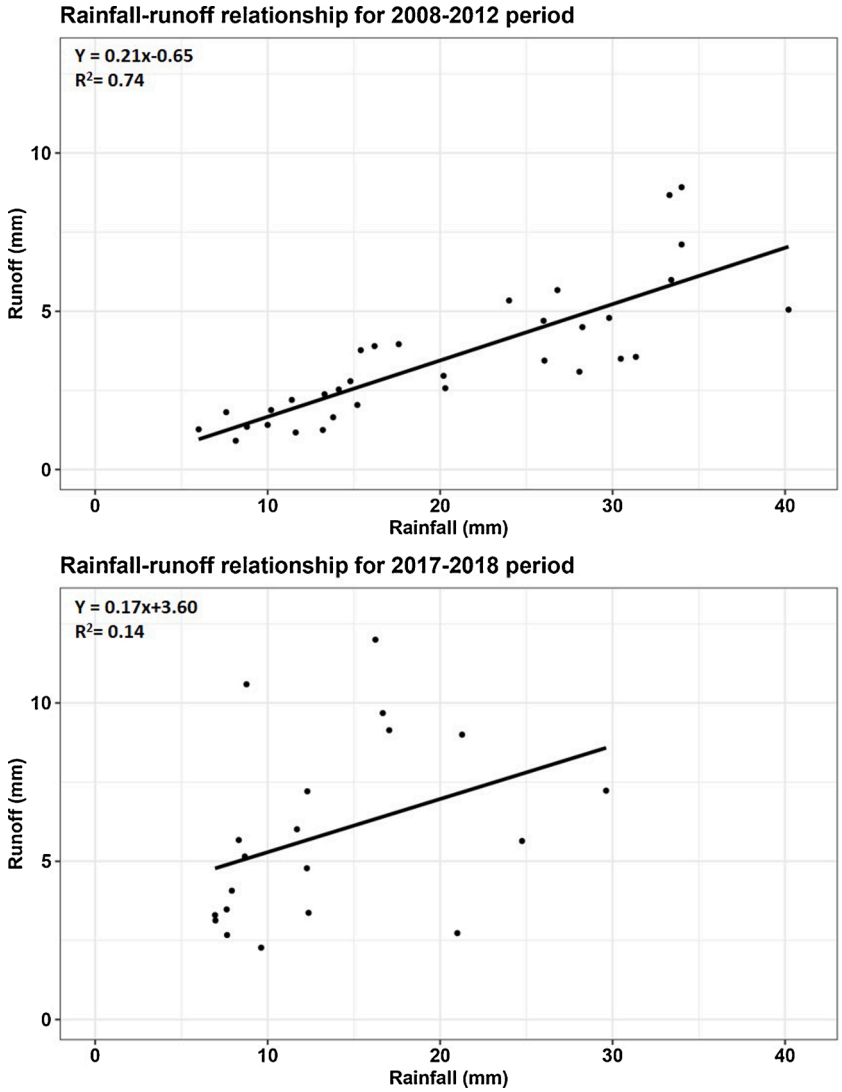

Fig. 4. Rainfall–runoff relationships in the urban sub-catchment Oued Fez for a) the 2008–2011 events, b) the 2017–2018 events.

2.3.1. The SCS production function

The first production function is the SCS (Soil Conservation Service-USDA, 1972), which has been widely used due to its simplicity in estimating the amount of rainfall contributed to the runoff (Michaud and Sorooshian, 1994; Hughes, 1994; Tramblay et al., 2010a, 2010b). In addition, it is well adapted to different types of flood generation processes (Steenhuis et al., 1995) and is still used to analyse the impact of urbanisation on runoff (Li et al., 2018). The SCS function gives an empirical relation between the depth of excess precipitation or direct runoff R (t) and the depth of precipitation P (t) after runoff begins (Chahinian et al., 2005).

In the ATHYS modelling platform, on each cell, the instantaneous version of the SCS model (Gaume et al., 2004) is used to divide rainfall into infiltrated/accumulated rain.

$$\mathrm{R}(t) = I(t) * \frac{P(t) - 0.2S}{P(t) + 0.8S} \cdot \left(2 - \frac{P(t) - 0.2S}{P(t) + 0.8S}\right) \tag{2}$$

Where

R(t): runoff at time t [$L.T^{-1}$]

I(t): rainfall intensity at time (t)[$L.T^{-1}$]

P(t): cumulated rainfall at time t [L]

S: maximum storage capacity of the reservoir assimilated to the soil [L]

S is likely to vary on an event basis according to the initial water deficit.

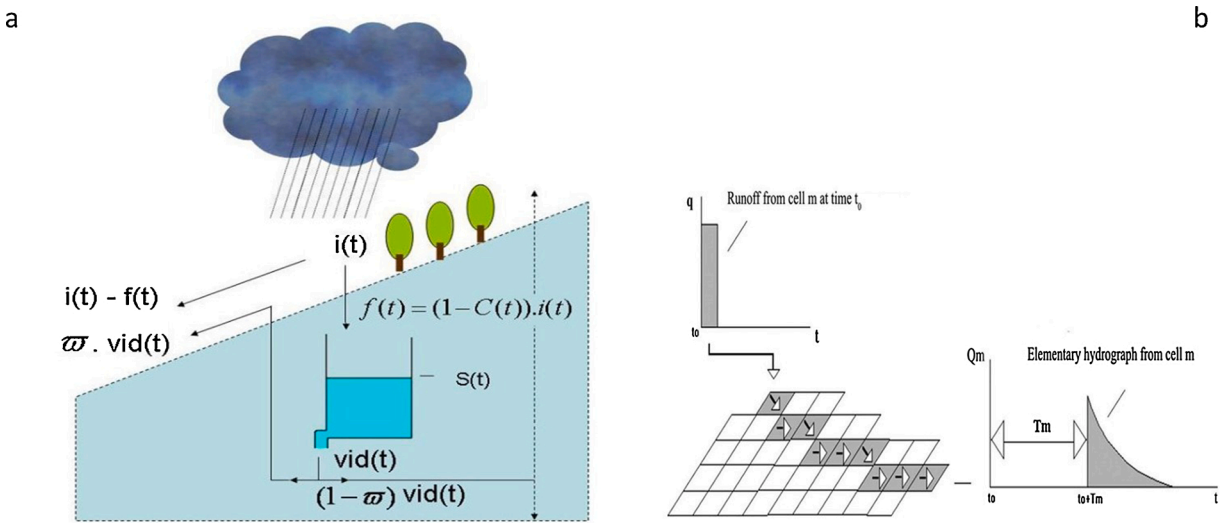

Fig. 5. a) The Soil Conservation Service (SCS) and b) lag & route models (from www.athys-soft.org).

2.3.2. *The variable runoff coefficient production function (Reservoir3)*

Reservoir3 is a specific production model implemented in ATHYS. It consists of a single linear reservoir and draws its name from the fact that it is the third reservoir model of the ATHYS environment and is referenced under this name in the graphical user interface. The model assumes a constant initial abstraction and an infiltration capacity that varies based on the reservoir's fill level.

$$\mathrm{R}(t) = [I(t) - INF] * \frac{S(t)}{STO} \; if \; I(t) > INF \tag{3}$$

$$\text{Else } \mathrm{R}(t) = 0 \tag{4}$$

Where

S(t) : water level in the reservoir level at time t [L]

STO: maximum reservoir capacity [L]

INF: constant infiltration capacity [$L.T^{-1}$]

For both functions, sub-surface flow ($Q_{sub}(t)$) is calculated as a portion of the linear reservoir's drainage loss (Eq. (5)) and added to the calculated runoff in order to obtain the total runoff produced by a cell.

$$Q_{sub}(t) = \varpi.\mathrm{ds} * \mathrm{S(t)} \tag{5}$$

ω: drainage fraction contributing to runoff, varies between 0 and 1 [-]

ds: exponential drainage coefficient [T^{-1}]

2.3.3. *The transfer function*

The runoff produced by the cell is transferred to the outlet using the lag and route transfer function (LR), which calculates an elementary hydrograph for each cell (Lhomme et al., 2004).

$$T_m = \sum_k \frac{V_k}{l_k} \tag{6}$$

$$K_m = K_0 . T_m \tag{7}$$

$$Qm(t) = A. \int_{t_0}^{t-\tau_m} \frac{P_n(\tau)}{K_m} exp\left(- \frac{t - t_0 - T_m - \tau}{K_m} \right) d\tau \tag{8}$$

Where

A: cell area [L^2]

T_m: routing time [T]

K_m: lag time [T]

L_k: length of each "k" cell, between cell "m" and the outlet[L]

V_k: flow velocity on each "k" cell[$L.T^{-1}$]

K_0: linearity coefficient between K_m and T_m[-]
t: time rainfall begins [T]

The elementary hydrographs are added up to obtain the full event hydrograph for the catchment outlet (Fig. 5b). This conceptual model is a generalisation of the unit hydrograph to a grid structure and is considered as a good approximation of the transfer process with lower calculation times.

Two formulations are used to determine the flow velocity (Bouvier et al., 2018).

- When assuming a constant velocity,

$$V_k = V_0 \text{ for all cells} \quad (9)$$

The transfer function's parameters are a velocity V_0 and a diffusion coefficient K_0.

- When assuming a geomorphological formulation, the velocity may be related to the slope and the area drained by the cell.

$$V_k = V_0.I^{\alpha}.S^{\beta} \quad (10)$$

Where
I: slope of the cell [$L.L^{-1}$]
S: upstream drained area of the cell [L^2]
α, β: empirical parameters [-]

In this study, we assume constant velocity and use the first formulation. This model does not take into account storage reservoirs such as lakes and dams since the transfer of the effective rainfall produced by each cell to the outlet is added individually.

2.4. Sensitivity analysis of the selected models

A basic sensitivity analysis was carried and two parameters were found to be sensitive for SCS-LR and three for Reservoir3-LR (Table 4a and 4b). The methodology consists in running simulations while modifying the set parameter values by ± 25 %, 50 % and 75 % as carried out in Fleischmann et al. (2018) and Samadi et al. (2019). The event of 01/05/2011 with a reference set of parameters for SCS-LR (S =35 mm; w = 0.20; ds = 4 day^{-1}; V_0 = 2.90 $m.s^{-1}$ and K_0 = 0.70) and Reservoir3-LR (STO = 30 mm; INF =2

Table 4a
Results of the sensitivity analysis for the SCS-LR model. The initial values are S =35 mm; w = 0.2; ds = 4 day^{-1}; V_0 = 2.9 $m.s^{-1}$ and K_0 = 0.7.

Parameter	% Variation		
	Value	Runoff	Peak flow
S (mm)	−75	−66	−75
	−50	−47	−60
	−25	−25	−38
	25	21	63
	50	29	103
	75	31	107
ω (−)	−75	60	42
	−50	56	25
	−25	22	11
	25	−15	−9
	50	−27	−17
	75	−35	−23
ds (day^{-1})	−75	39	21
	−50	16	12
	−25	6	5
	25	−3	−4
	50	−6	−7
	75	−8	−10
V_0 ($m.s^{-1}$)	−75	55	127
	−50	11	63
	−25	3	36
	25	−1	−7
	50	−2	−7
	75	−3	−2
K_0 (-)	−75	−2	−19
	−50	2	17
	−25	−1	−8
	25	1	8
	50	−1	−15
	75	3	25

mm.h^{-1}; w = 0.20; ds = 4 day^{-1}; V_0 = 2.70 m.s^{-1} and K_0 = 0.70) was chosen for the sensitivity test. Only one parameter per run was tested, and the remaining ones were set to fixed values throughout the runs.

The sensitivity results for model parameters with regard to runoff volume (Vr) and peak flows (Qp) for SCS-LR and Reservoir3-LR are presented in Table 4a and 4b. It can be seen that for SCS-LR, S has the greatest influence on the runoff volume and peak flow, as a 25 % increase in parameter S induces 21 % and 63 % variation on these variables, respectively. The same increase in parameter ds induces 3% variation in volume and 4% in peak flow, while for parameter ω the variation is by 22 % and 11 % respectively. Note that setting ω = 0 would lead to no drainage uptake, while ω = 1 would lead to total drainage uptake. The parameters of the transfer function have a slight impact on the volume but a greater influence on the peak flow. In this regard, V_0 is more sensitive than K_0: a 25 % decrease in both induces 3% variation in volume and 36 % in peak flow for V_0 and respectively -1% and 8% for K_0. The results of the sensitivity analysis of the SCS-LR model are in accordance with those of Nguyen and Bouvier (2019).

For the Reservoir3-LR model (Table 4b) of all the parameters of the production function, STO has the greatest impact on the peak flow, a 25 % decrease in the value of STO induces 16 % variation in the simulated peak flow. ω and ds yield important variations in volume since they control reservoir drainage and uptake: a 25 % decrease in ω yields 24 % variation in the volume and 12 % in the peak flow. However, on impervious surfaces, the possibility of drainage uptake is slim. The results for the transfer function remain unchanged, i.e. V_0 is more sensitive than K_0.

Based on the sensitivity analysis results, it was decided to calibrate S and V_0 for the SCS-LR model and STO and V_0 for the Reservoir3-LR model. Since we had no prior knowledge of the value of the parameter INF, we resorted to calibrating it as well. The remaining parameters were set to ω = 0, ds = 4 day^{-1} and K_0 = 0.70.

2.5. The parametrisation schemes

2.5.1. Extracting the drainage network

The "Advanced Land Observing Satellite - Phased Array type L-band Synthetic Aperture Radar Radiometric Terrain Correction" (ALOS PALSAR RTC, https://asf.alaska.edu/data-sets/sar-data-sets/alos-palsar/) high-resolution digital elevation model (DEM) with a

Table 4b
Results of the sensitivity analysis for the Reservoir3-LR. The initial values are STO = 30 mm; INF =2 mm.h^{-1}; w = 0.2; ds = 4 day^{-1}; V_0 = 2.7 m.s^{-1} and K_0 = 0.7.

Parameter	% Variation		
	Value	Runoff	Peak flow
STO (mm)	−75	−36	−62
	−50	−16	−36
	−25	−6	−16
	25	4	13
	50	7	23
	75	9	32
INF (mm. h^{-1})	−75	−16	−29
	−50	−9	−21
	−25	−4	−12
	25	5	16
	50	10	38
	75	23	70
ω (−)	−75	32	29
	−50	30	27
	−25	24	12
	25	−16	−10
	50	−28	−17
	75	−37	−24
ds (day^{-1})	−75	35	7
	−50	20	−7
	−25	8	−6
	25	−7	7
	50	−12	15
	75	−17	24
V_0 (m.s^{-1})	−75	66	131
	−50	14	62
	−25	4	34
	25	−1	−8
	50	−2	−10
	75	−3	−8
K_0 (-)	−75	−3	−22
	−50	−3	−20
	−25	−2	−15
	25	−1	−4
	50	−1	3
	75	−4	9

12.5-metre resolution is used to generate the natural drainage network using ATHYS's in-built extraction procedure. ALOS PALSAR was selected because several studies found it to perform better than other open-source DEMs (Ali et al., 2012; Courty et al., 2019; Ngula Niipele and Chen, 2019).

The DEM is first resampled at 10 m spatial resolution and then used to determine the natural drainage network using the D8 algorithm (O'Callaghan and Mark, 1984; Tarboton et al., 1991) built into ATHYS. Once pits are removed, the drainage direction of each cell is determined based on the steepest slope, and the flow accumulation is calculated. The network corresponding to a 10 ha flow accumulation threshold is extracted and corrected using the 1:25000 scale topographic maps. This drainage network will be referred to as natural drainage (ND).

A map of the street network is used to force the drainage directions along the motorways. The street network is really dense in the old Medina and Fez Jedid sectors, with very narrow pedestrian streets that cannot be mapped correctly at the scale we worked at. Hence, we used the road network, i.e. streets that could be travelled by motor vehicles. This network was burned into the DEM by reducing the elevation of the cells on which this artificial network is located, as carried out by Rodriguez et al. (2000) and Gironas et al. (2010), and a new drainage network was extracted. This drainage network will be referred to as the modified drainage network (MD) (Fig. 6). Note that the model is fully gridded with independent cells, i.e., each cell produces an elementary hydrograph. By modifying the drainage directions, the distance to the outlet (or length L_k) and the upstream drained area by the cell will be modified (Fig. 7). However, since we use the simple formulation of the transfer function (Eq. (9)), only the change in distance will directly impact our results. The simple formulation is not impacted by the changes in slope value either.

When comparing the distributions of L_k for both drainage models (Fig. 7), it can be seen that by adding the road network, new, shorter connections are created, resulting in a decrease of the maximum L_k value from 1066 m (ND) to 866 m (MD) and a shift in the median L_k value, which moves from 583 m to 444 m. The 1st and 3rd quantiles are also lower: 270 m and 607 m for MD as opposed to 368 m and 775 m for ND.

2.5.2. *Spatial discretisation*

In order to represent the effect of urbanisation on runoff generation, we have divided the urban area of the Oued Fez catchment into production classes based on land use (Fig. 1b). Two land use maps were created using Google Earth Images from 2008 and 2017. The first one was used for the 2008–2012 period and the second one for the 2017–2018 period. The urban sprawl corresponds to a total area of 7.80 km^2 and is mostly concentrated in the peri-urban area located in the southern part of the catchment, namely around the districts of Ain Chkef and Ouled Tayeb (Fig. 1b). According to official sources, the development of Ain Chkef has increased by 0.33 % between 2007 and 2014 and 40 % of the housing in Ouled Tayeb was built after 2009 (MATNUHPV, 2019). Hence, the potential errors in land use type for the 2011–2012 events do not concern the more densely built areas, whose limits have been stable throughout the

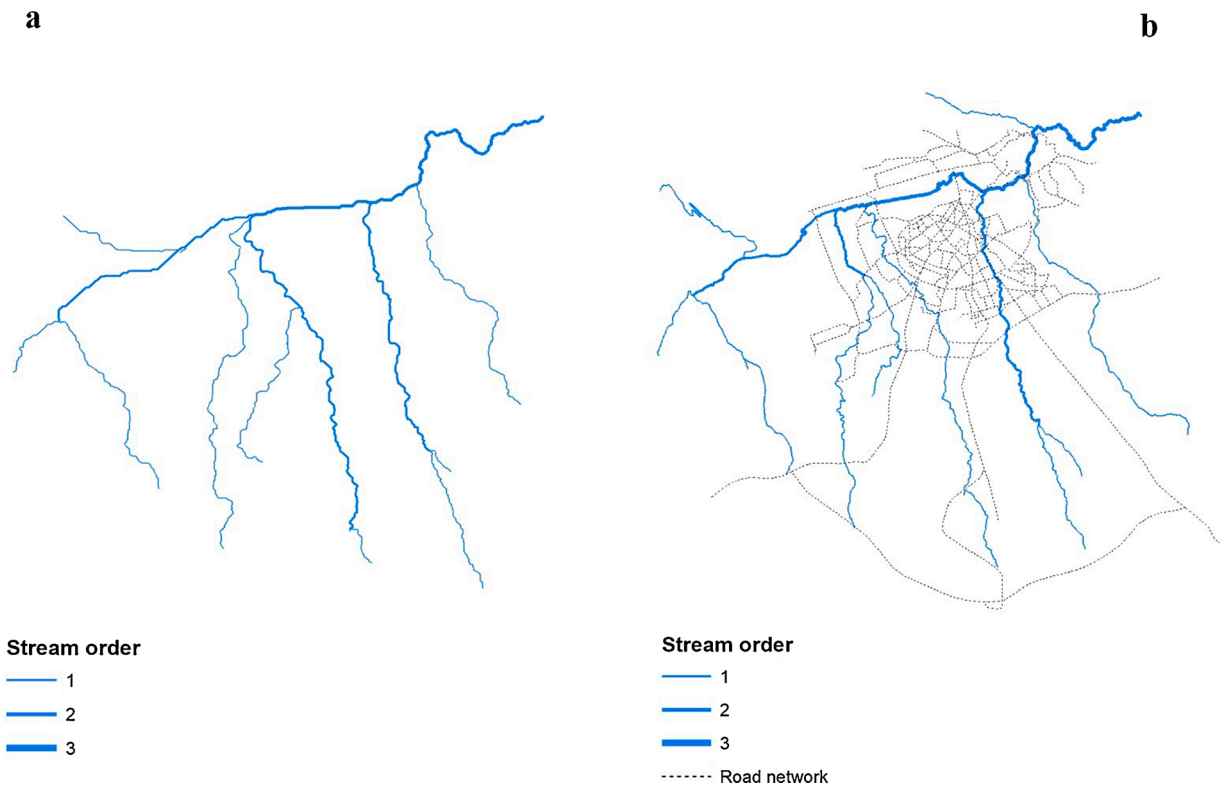

Fig. 6. Drainage networks represented for an upstream drained area of 10 ha: a) natural network (ND); b) network with burnt street network (MD).

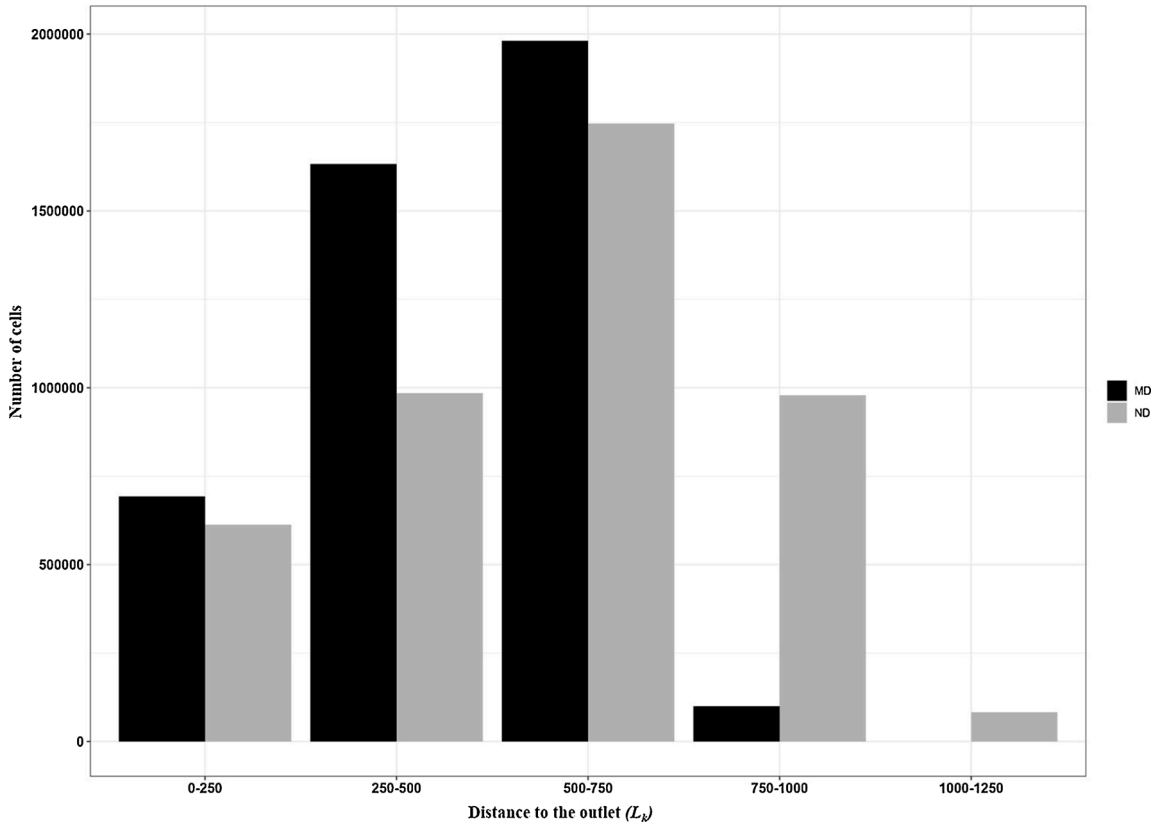

Fig. 7. Histograms of cell distance to the outlet (L_k) for the natural network (ND) and the modified network (MD).

study period, but rather the peri-urban areas whose impervious surfaces may be over-estimated. Between 2008 and 2012, the building permits granted by the state amounted to a total built area of 1.10 km^2 excluding roads built by the government (Haut Commissariat au Plan, 2020). Hence, by using the 2008 land use maps for the 2011–2012 events, the value of parameter S might be over-estimated for these plots. We started with six classes and, after some primary tests, decided to reduce them to three as a compromise between over-parametrisation and representativeness. This is in accordance with Jakeman and Hornberger (1993), who assume that five parameters should be sufficient to reproduce hydrological processes. Of course, the number of parameters for accurate representation of the hydrological processes is model-based and high-capacity computers nowadays remove some of the limitations that were common in the early days of distributed hydrological modelling. However, hydrological systems are highly non-linear with threshold effects. On catchments with limited data, it would still be difficult to correctly calibrate a large number of parameters without getting into equifinality problems.

The three classes are:

- The ZA class: corresponds to agricultural and natural areas.
- The ZU class: corresponds to urban areas formed by isolated dwellings or buildings.
- The ZUD class: corresponds to densely urbanised areas such as the old Medina and Aouinat El Hajaj districts.

Table 5
Synthetic table of the parameterisation and calibration procedure.

Symbol	Description	Units	Estimation method	Spatial variability
S	Maximum storage capacity of the reservoir-soil	[mm]	Calibration	Yes
STO	Maximum reservoir capacity	[mm]	Calibration	Yes
INF	Constant infiltration capacity	[mm. h^{-1}]	Calibration	Yes
ω	Drainage fraction contributing to runoff	[-]	Fixed value, trial and error ($\omega = 0$)	No
ds	Exponential drainage coefficient	[day^{-1}]	Fixed value, trial and error ($ds = 4\ day^{-1}$)	No
K_0	Linearity coefficient between routing time and lag time	[-]	Fixed value based on literature * ($K_0 = 0.7$)	No
V_0	Flow velocity	[$m.s^{-1}$]	Calibration	No

* Bouvier et al., 2018.

For each model, three sets of parameters, corresponding to the three land use classes are calibrated for the production function (Table 5). The parameters to be calibrated are: S for the SCS model and INF and STO for the Reservoir3 model. For both models, ω and ds are set to default values of 0 and 4 day^{-1}. For the transfer function, parameter V_0 is calibrated and K_0 is set to 0.70. Two values of V_0 are calibrated, one using the natural drainage network (ND) and one using the modified drainage network (MD). Calibration is carried out using the model's in-built automatic calibration procedure based on the simplex algorithm on each event of the calibration set independently.

Rainfall is interpolated using Thiessen polygons. No rainfall and runoff data are available on the upstream part of the catchment, which is mostly rural anyway. Given its karstic nature, we assumed that this zone's direct contribution to the runoff at the catchment outlet is insignificant at the event time scale (mean duration =880 min). It contributes mainly through springs, which already pour into the river network and are accounted for indirectly. This assumption will have to be revised in the future in light of new experimental data.

2.6. Model calibration and validation

The coupled SCS-LR and Reservoir3-LR models of the ATHYS platform are tested on the peri-urban and urban parts of Oued Fez in event-based mode at hourly and sub-hourly time steps.

The split sample test procedure (Klemeš, 1986) is used and the flood events recorded over the entire study period are divided into two sets randomly. The first one is used to calibrate the models' parameters, while the second one is used to verify the reproducibility of the results and to assess the representativeness of the calibrated parameter sets (validation). The median value of the calibrated parameters is used to simulate the events of the validation set.

The Nash and Sutcliffe efficiency measure (NSE-Nash and Sutcliffe, 1970) is used to assess the models' ability to reproduce the observed flood hydrographs. In addition, the RMSE is used to quantify the errors on peak flows and runoff volumes.

$$NSE = 1 - \frac{\sum_{i=1}^{N} (Qsim_i - Qobs_i)^2}{\sum_{i=1}^{N} \left(Qsim_i - \overline{Q\ obs}\right)^2} \tag{11}$$

$$RMSE = \sqrt{\frac{\sum_{i=1}^{N} (V_{sim} - V_{obs})^2}{N}} \tag{12}$$

Where

Q_{sim}: simulated discharge for the event [LT^{-1}]
$Q_{obs:}$ observed discharge for the event [LT^{-1}]
$\overline{\overline{Q}}_{obs}$: mean observed discharge for the event [LT^{-1}]
V_{sim}: simulated volume for the event [LT^{-1}]
V_{obs}: observed volume for the event [LT^{-1}]

3. Results

The optimal values of the calibrated parameters for SCS-LRn, Reservoir3-LRn, SCS-LRm and Reservoir3-LRm are listed in Tables 6a, 6b and 7a, 7b. Table 6a and 6b present the median values of the calibrated parameters at hourly time steps. It can be seen that the maximum retention capacity of the soil reservoir S for the SCS-LR model and the reservoir capacity STO for the Reservoir3-LR model, are variable. The minimum values of S are obtained for the ZUD class, which corresponds to densely urbanised areas. This suggests that densely urbanised areas are highly impervious and infiltration is very low. The maximum values are obtained for the ZA class, which corresponds to agricultural areas characterised by a high infiltration capacity: the median parameter values are nearly double those of the urban areas, i.e., in comparison with agricultural areas, retention is reduced by a factor of two in urban areas.

We can further observe that the median values of both S and STO when using a modified drainage network are slightly lower than those obtained when using a natural network. This can be explained by the fact that taking into account urbanisation has contributed to an increase in surface runoff and a decrease in infiltration capacity, as highlighted also by several studies such as (Miller et al., 2014) and Xu and Zhao (2016).

Table 7a and 7b present the median values of the calibrated parameters at 5-minute time steps. It shows similar trends to those

Table 6a
Median values of the calibrated parameters for the SCS-LR models at hourly time step.

	S (mm)			Vo ($m.s^{-1}$)
	ZA	ZUD	ZU	
SCS-LRn	82	1.30	28	3.54
SCS-LRm	77	1.25	26	3.55

Table 6b
Median values of the calibrated parameters for the Reservoir3-LR models at hourly time step.

	STO (mm)			INF (mm. h^{-1})			Vo ($m.s^{-1}$)
	ZA	ZUD	ZU	ZA	ZUD	ZU	
Reservoir3-LRn	79	2.37	22	8.21	0.12	1.01	3.38
Reservoir3-LRm	78	1.39	20	8.04	0.10	1.03	3.59

Table 7a
Median values of the calibrated parameters for the SCS-LR models at 5-minute time step.

	S (mm)			Vo ($m.s^{-1}$)
	ZA	ZUD	ZU	
SCS-LRn	60	0.30	7	3.56
SCS-LRm	53	0.29	7	3.59

Table 7b
Median values of the calibrated parameters for the Reservoir3-LR models at 5-minute time step.

	STO (mm)			INF (mm. h^{-1})			Vo ($m.s^{-1}$)
	ZA	ZUD	ZU	ZA	ZUD	ZU	
Reservoir3-LRn	60	0.88	7	10	0.15	1.20	3.00
Reservoir3-LRm	59	0.77	6	10	0.20	1.00	3.79

found when calibrating events at an hourly time step, i.e., the minimum values of the production parameters S and STO correspond to the heavily urbanised areas, while agricultural areas are characterised by the highest values. The optimal values of the INF parameter for the Reservoir3 model are also lowest for the densely urbanised area class (ZUD) and highest for the agricultural zones class (ZA). Furthermore, no correlation was found between the calibrated values of parameter S and the classical previous 5-day antecedent rainfall at both time steps. At the hourly time step: $R^2 = 0.05$ for S(ZA) and $R^2 = 0.01$ S(ZU) for the SCS-LRn model, and $R^2 = 0.02$ and $R^2 = 0.01$ for the SCS-LRm model. At the 5-minute time step: $R^2 = 0.14$ for S(ZA) and $R^2 = 0.17$ S(ZU) for the SCS-LRn model, and $R^2 = 0.16$ for S(ZA) and $R^2 = 0.12$ for S(ZU) for SCS-LRm.

The maximum velocity reached at the outlet (V_0) is characterised by a slight inter-event variation, as also highlighted by Laganier et al. (2014), who indicated that the V_0 values are variable, but consistent with the commonly observed velocities. By analysing the calibrated values of the V_0 parameter, it can be seen that the minimum values are obtained for low- intensity events while high-intensity events were characterised by the greatest values.

We further investigated parameter changes across time periods for both time steps (Tables 6a, 6b and 7a, 7b). A decrease in the S and STO parameter values and an increase in the V_0 parameter values can be observed between 2011/2012 and 2017/2018. These changes are thought to be due to an increase in the channelisation of the hydrographic network as well as an increase in the urbanisation of the catchment.

3.1. Evaluation of the models' performance at different time steps

3.1.1. Calibration phase

The investigation of the models' performance is based on the Nash and Sutcliffe criterion (NSE is presented in Fig. 8). The boxplots represent the distribution of the criterion for the hourly data (2008–2018, 26 events) and 5-minute time steps (2011–2018 data, 17 events). They indicate that the results of the simulations are not spread out.

At the hourly time step, the median NSE values range between 0.73 and 0.85 and the percentage of events having NSE > 0.6 varies from 84 % to 88 %. Thus, the models' performance can be considered satisfactory. When comparing the ranking of the four models, it can be seen that the SCS-LRm model is the most appropriate for the calibration database, while the Reservoir3-LRn model shows a lower performance and has the lowest NSE median values.

Flood event simulations at a finer time scale (5 min) were also carried out using flood events recorded during the 2011/2018 periods. The results indicate that all four models are able to reproduce the flood hydrographs correctly: the median NSE ranges between 0.51 and 0.69. For the SCS-LRm, 77 % of the events have NSE > 0.6. The percentage drops to 65 % for Reservoir3-LRm and 53 % for SCS-LRn. The lowest values are those of Reservoir3-LRn with 47 %. Similarly to the results obtained at the hourly time step, SCS-LRm outperforms the other three models.

The determination coefficient R^2 and the RMSE were used to judge the models' performance in terms of the runoff volume and peak flow restitution. The linear regressions between the observed and simulated flood events in terms of runoff volumes and peak flow are presented in Fig. 9a and b. A good correspondence can be seen between the observed and simulated runoff volumes for all tested models at the hourly time step (Fig. 9a), with R^2 varying between 0.97 and 0.98 and RMSE between 0.16 and 0.25. In terms of peak

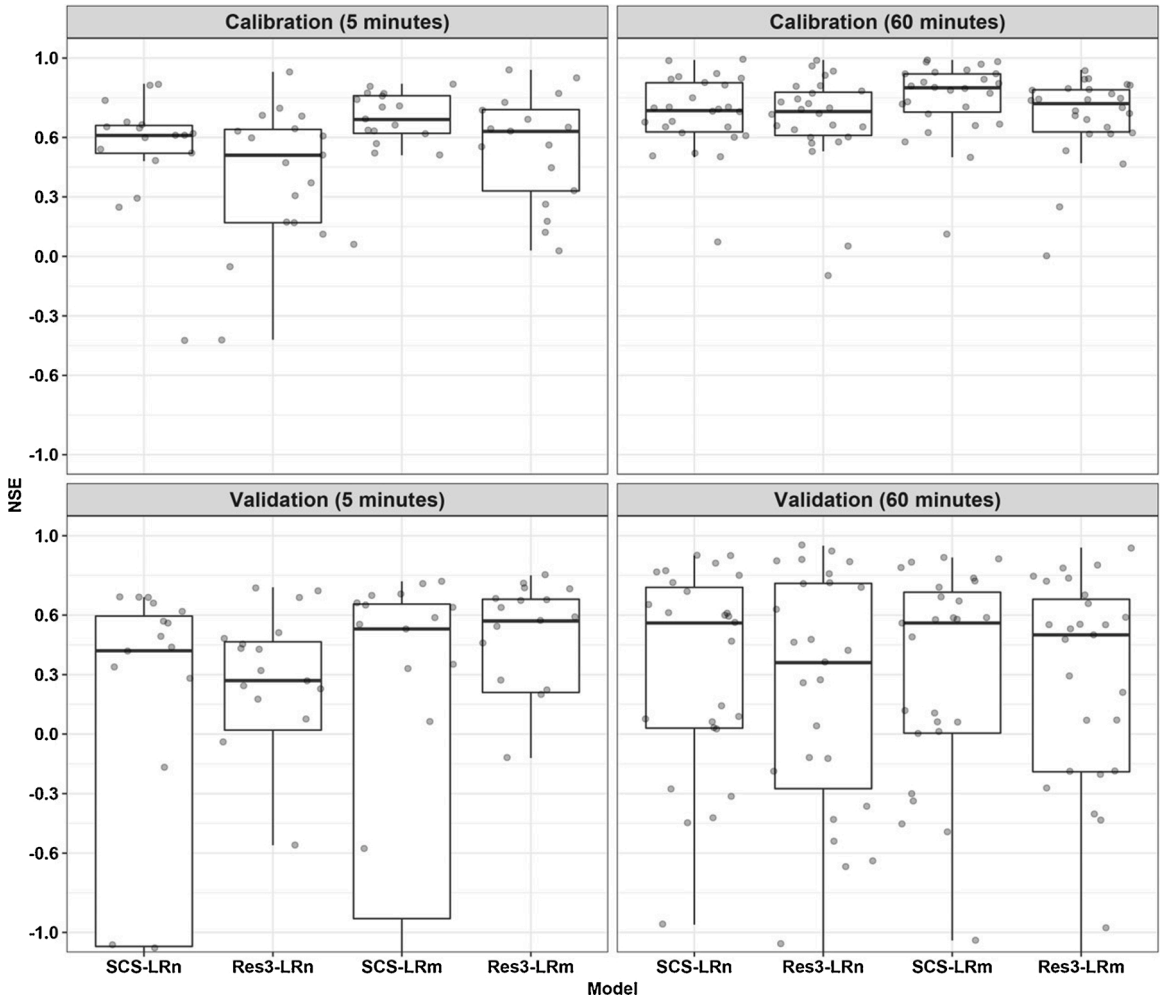

Fig. 8. Box plots of the NSE criterion for the calibration and validation events (hourly and 5-minute time steps).

flow, a good agreement can be noticed also between the two hydrographs, with R^2 varying between 0.88 and 0.93 and RMSE between 0.18 and 0.23. At the 5-minute time step (Fig. 9b and Table 8) the R^2 and RMSE values drop slightly for both volume (0.94 to 0.97 and 0.22 to 0.32, respectively) and peak flow (0.78 to 0.93 and 0.23 to 0.42). Visual comparison of the simulated and observed hydrographs (see examples in Fig. 10a and b) also shows a good agreement.

3.1.2. Validation phase

The median values of the calibrated parameters at different time steps (60 and 5 min) are used to simulate the validation events. Note that for the 5-minute time step only the 19 flood events recorded during the 2011/2012 and 2017/2018 periods are used. Based on the NSE criterion, the models' performance is degraded at the hourly time step: the median NSE values range between 0.39 and 0.56. Save for SCS-LRn and Reservoir3-LRn, the models give the same performance at the 5-minute time step, with the median NSE values varying between 0.27 and 0.57 (Fig. 8).

At the hourly time step, the models' ranking remains unchanged: 45 % of the flood events simulated by the SCS-LRm model have an NSE value > 0.6. The percentage drops to 34 % for Reservoir3-LRn and rises to 37 % for Reservoir3-LRm. The models' ranking is unchanged at the 5-minute time step: for SCS-LRm 47 % of events have an NSE > 0.6, 42 % for Reservoir3-LRm, 35 % for SCS-LRn and 12 % for Reservoir3-LRn.

Similar performances are obtained when looking at the runoff volume and peak flow simulation at both time steps (Fig. 9 and Table 8). At the hourly time step, the R^2 and RMSE for the runoff volume range between 0.23 to 0.37 and 58 to 0.63 and between 0.19 to 0.41 and 0.53 to 0.69, respectively, for peak flow. For the 5-minute time step, they drop to 0.13 to 0.69 and 0.31 to 0.87, respectively, for volume and 0.17 to 0.50 and 0.45 to 0.61 for peak flow. The performance is slightly degraded in both calibration and validation when reducing the modelling time step (Fig. 9b). Ficchi et al. (2016) found similar results and stated that although the performance of the tested model was greatly improved when changing from a 1- day to a 6-h time step, a reverse trend was found when decreasing the time step from 1 h to 6 min. The same study showed that reducing the time step has the opposite effect under high flow

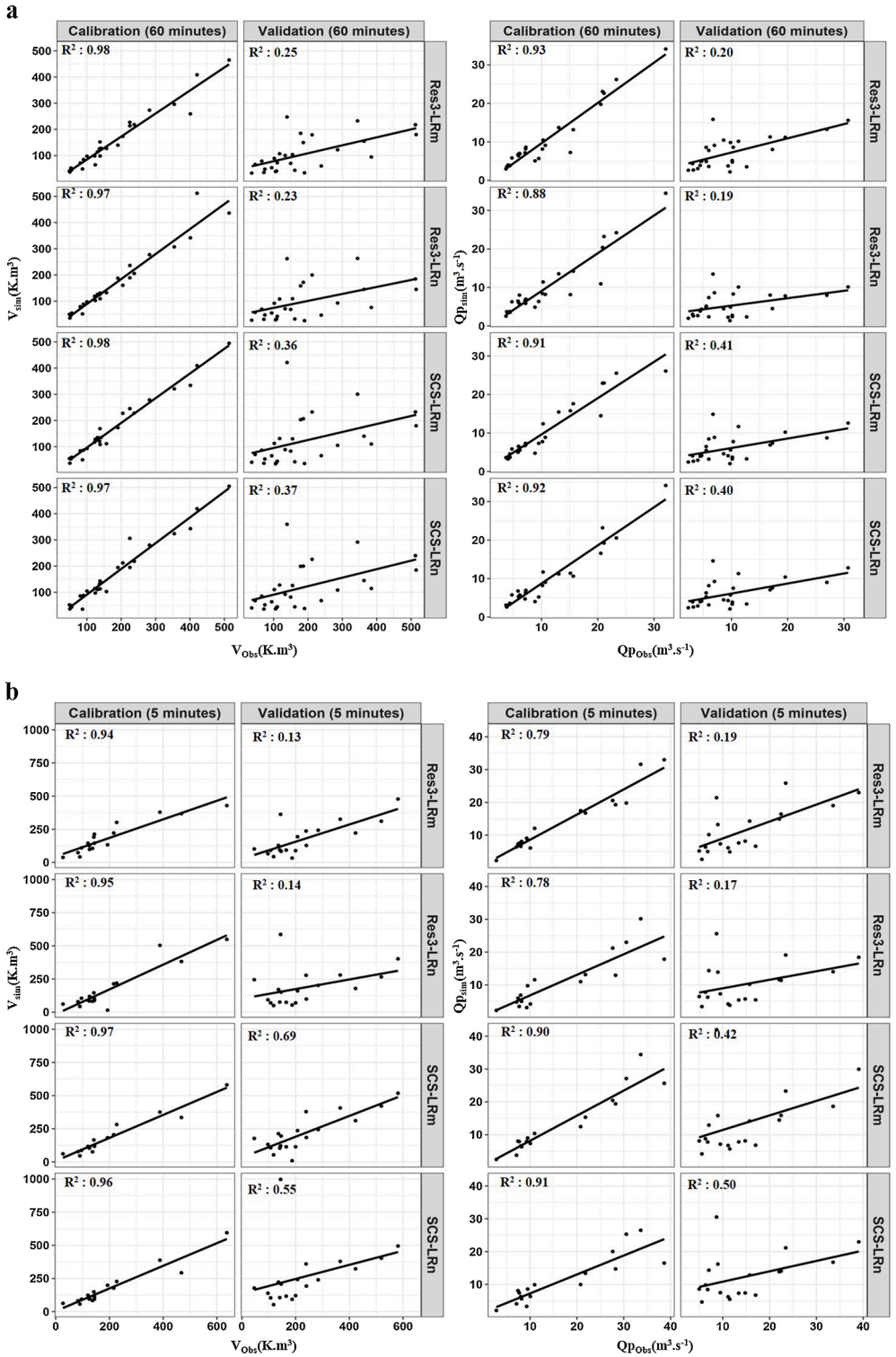

Fig. 9. Observed (Qpobs) and calculated (Qpsim) peak discharges and observed (Vobs) and simulated (Vsim) runoff volume for the calibration and validation events a) at hourly time step and b) at 5-minute time step.

conditions. This finding is consistent with our results, as the rainfall–runoff events simulated at the 5-minute time step are characterised by higher flow conditions than those modelled at an hourly time step.

The models' capacity to reproduce the catchment's hydrological response was assessed by analysing the relationship between

Table 8
RMSE values for calibration and validation periods (hourly and 5-minute time steps).

Hydrological models	Calibration period (hourly) RMSE (Vr)	Validation period (hourly) RMSE (Qp)	Calibration period (5-minute) RMSE (Vr)	Validation period (5-minute) RMSE (Qp)	RMSE (Vr)	RMSE (Qp)	RMSE (Vr)	RMSE (Qp)
SCS-LRn	0.16	0.19	0.58	0.61	0.32	0.41	0.87	0.56
Reservoir3-LRn	0.19	0.23	0.63	0.69	0.22	0.42	0.62	0.60
SCS-LRm	0.18	0.19	0.61	0.62	0.25	0.27	0.31	0.61
Reservoir3-LRm	0.25	0.18	0.58	0.53	0.23	0.23	0.41	0.45

rainfall and simulated runoff for all events (Fig. 11). This analysis was carried out at an hourly time step to be able to use the largest available dataset. It can be seen that the linear relationship is correctly reproduced for the 2008–2011 events, with slightly higher values for the correlation coefficient ($0.81 \leq R^2 \leq 0.85$) and, save for the Reservoir3-LRm model, similar values for the slope of the regression line ($0.20 \leq a \leq 0.22$). The non-linear relationship of the 2017–2018 events is also reproduced, with even lower values for the correlation coefficient ($0.07 \leq R^2 \leq 0.23$).

All criteria and time steps considered, the models' performance in validation is poor. The models' lack of robustness is increased by the change in the rainfall–runoff relationship on the catchment (Fig. 4) throughout the study period. On the one hand, 2008–2009 was an exceptionally wet year (annual rainfall of 810 mm vs 523 mm for 2017–2018) and on the other the flow conditions on the catchment were modified, as highlighted by the experimental data (Fig. 4) and the observations made in the field regarding the extension of the stormwater and wastewater networks. By calibrating and validating the models within and not across the periods, i.e., using the median of the parameters for each period, better results are obtained: at the hourly time step the median NSE values range between 0.61 and 0.74 and at the 5-minute time step between 0.48 and 0.62.

3.2. Effect of rain gauge network density and rainfall event type on the models' performance

The modelling results were further investigated to highlight any possible effect of the rain gauge network density on the models' performance. The rainfall events were divided into two groups: single gauge events, i.e. events recorded when only a single rain gauge was implemented, and multiple gauge events, i.e. events recorded when two or more rain gauges were implemented. The analysis was only carried out at the hourly time step because our database did not contain any single gauge events at the 5-minute time step and only 5 events for which rainfall was measured using two gauges. When examining the models' results based on the rain gauge density using the NSE criterion, it was found that, for the calibration phase, all the tested models reproduce the observed hydrographs well when rainfall information is provided by two or four rain gauges (Fig. 12a). The median NSE value of the four models ranges between 0.62 and 0.72 for the events where rainfall information is obtained using a single gauge, and between 0.74 and 0.89 when using multiple rain gauges. The results are poorer for the validation phase, where the models' performance is lower for the events where the rainfall information was provided by multiple rain gauges. However, this is not thought to be due to the rainfall information but rather to the models' lack of robustness and overall poor performance in validation. As can be seen in Table 3, all the events for which rainfall information is provided by a single rain gauge belong to the 2008/2012 period, while nearly all the events for which rainfall information is provided by multiple rain gauges belong to the 2017/2018 period. Thus, the median values of the calibrated parameters converge towards the optimum values of the 2008/2012 period, which constitutes 65 % of the total number of events in our database.

We further wanted to investigate the influence of the rainfall type. We used the 75th and 25th percentiles value of total rainfall to separate the events. All events where the total rainfall was below the 25th percentile were considered as low rainfall events and those where the total rainfall was above the 75th percentile were considered as high rainfall events.

The results at the hourly time step (Fig. 12b), both in calibration and validation, indicate that the selected models are able to reproduce the high rainfall events ($0.72 <$ NSE median < 0.78) and perform less well on low rainfall events ($0.63 <$ NSE median <0.89). The findings are similar at the 5-minute time step despite the lower NSE thresholds, i.e. $0.54 <$ NSE < 0.72 for high rainfall events as opposed to low rainfall events $0.27 <$ NSE < 0.54. Note that NSE is known to be more sensitive to high flow values (Tegegne et al., 2017).

4. Discussion

The analysis of the calibrated parameters at the hourly time step indicates that the median values of parameter S for urban areas is 28 mm using the SCS-LRn model and 26 mm for the SCS-LRm model. These results are in the same range as those reported by Bouvier et al. (2018) on the Ouagadougou metropolitan area. The S values calibrated for the agricultural zones are consistent with those of Laganier et al. (2014), who identified similar variation trends on the predominantly rural Anduze catchment ($108 < S < 408$ mm).

The values of the transfer parameter V_0, however, are slightly higher than those obtained by Tramblay et al. (2010a, 2010b), Laganier et al. (2014) and Coustau et al. (2012). They are in the same order of magnitude as those obtained by Tramblay et al. (2011), who showed that V_0 tends to increase when using uniform rainfall as opposed to when using spatially distributed rainfall inputs. Arnaud et al. (2002) also indicate that the calibration of rainfall–runoff models is impacted by uniform rainfall. Our results show that the median V_o value for the tested models varies between 3.24 $m.s^{-1}$ and 4 $m.s^{-1}$ when the rainfall information comes from one rain gauge and ranges between 3.11 $m.s^{-1}$ and 3.50 $m.s^{-1}$ when the rainfall is provided by four rain gauges. These values can also be partly

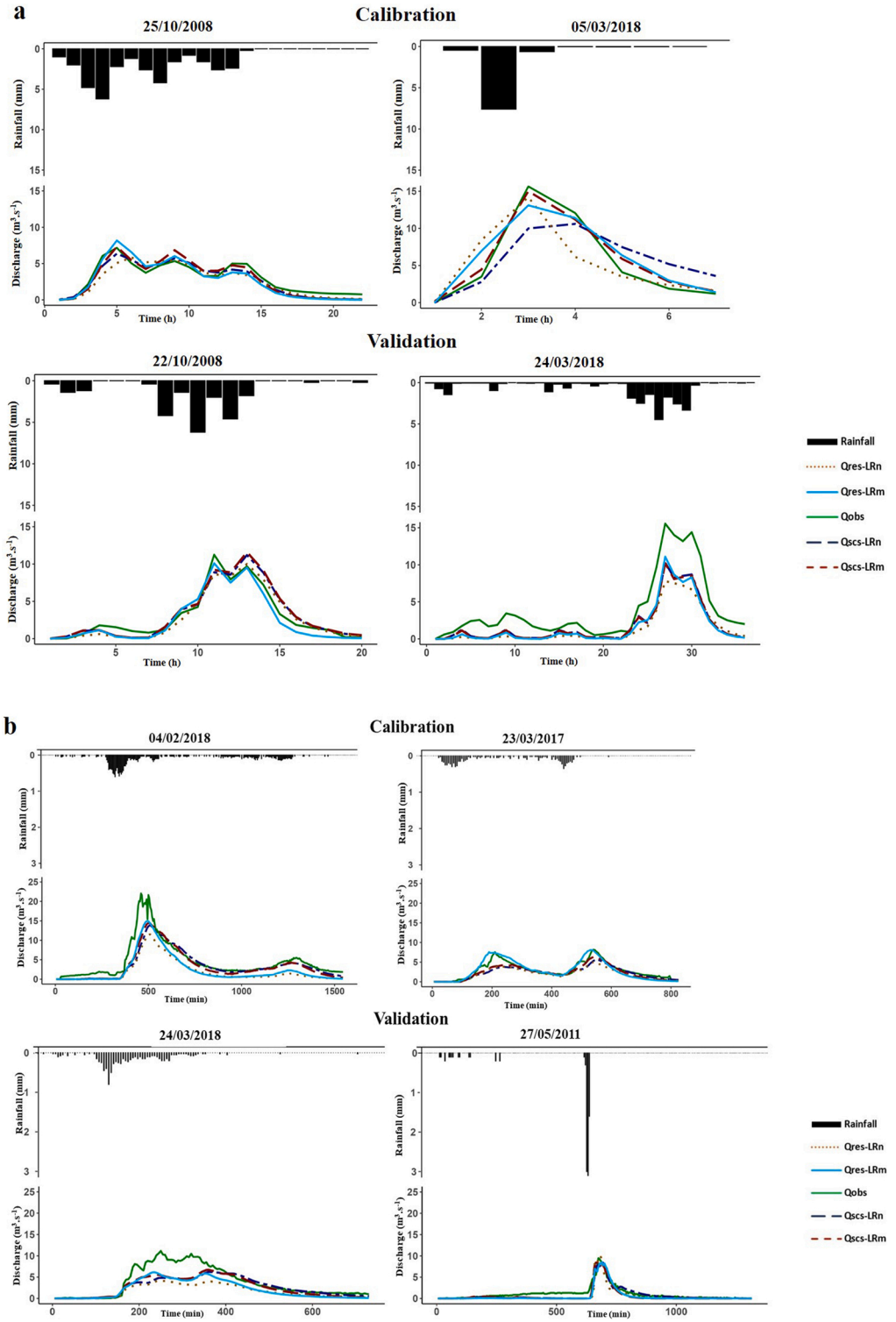

Fig. 10. Simulated hydrographs of some calibration and validation events a) at hourly time step and b) at 5-minute time step.

explained by the urban nature of our catchment: V_0 has slightly higher values when using the modified drainage network (MD) as input for the Reservoir3 model than when using the natural drainage network (ND) at both time steps. This can be explained by the configuration of the modified drainage (MD). By adding the road network, shorter connections are created between the cells and the distances to the outlet (L_k) are decreased (Fig. 7). In order to maintain the same routing time (Tm), the velocity (V_k) will have to slightly

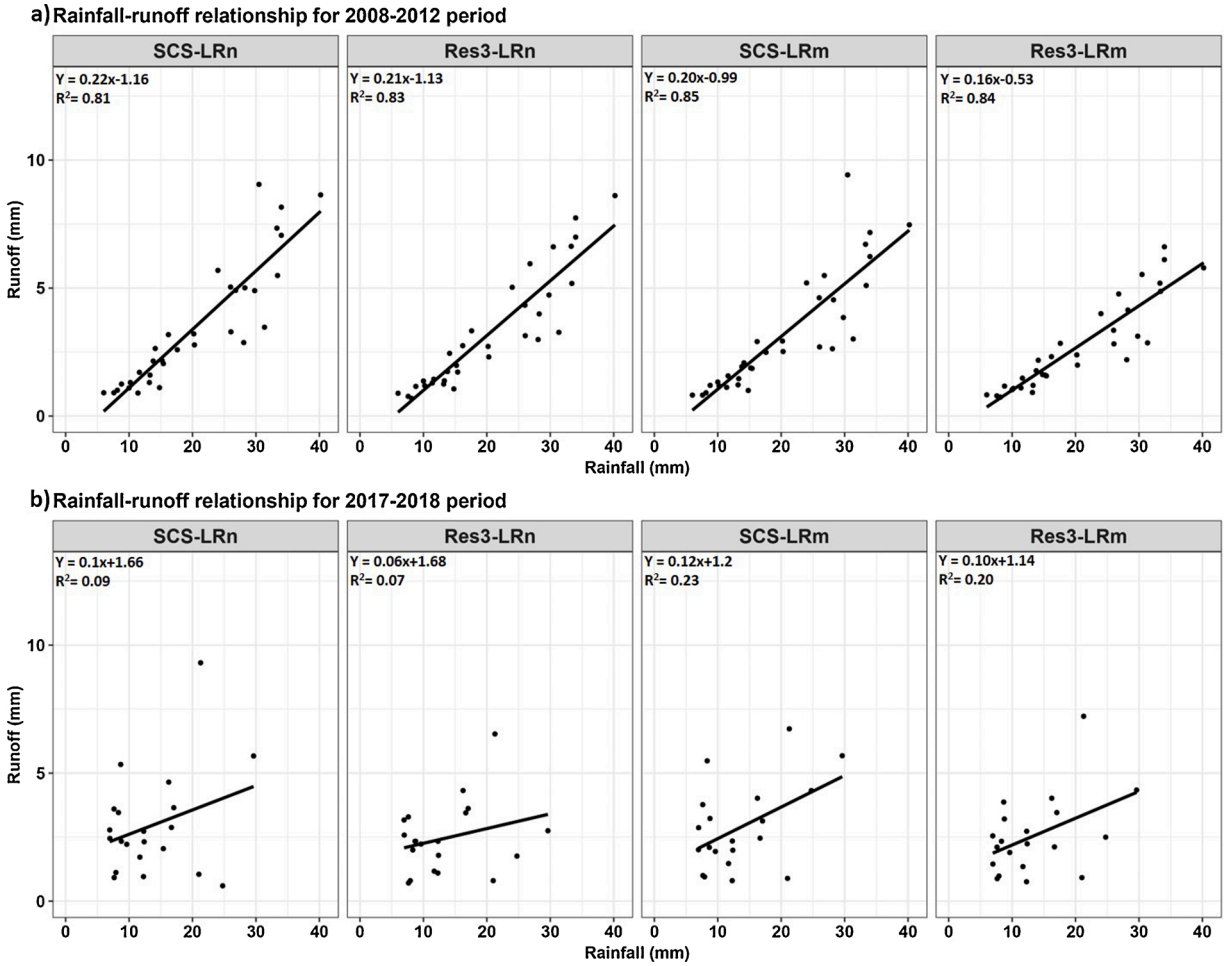

Fig. 11. Simulated runoff vs rainfall for the calibration and validation events at hourly time step a) for the 2008–2012 period and b) for the 2017–2018 period.

increase.

When analysing the V_0 values, it can be noticed that the flood events that belong to the 2017–2018 period are characterised by relatively high V_0 values compared to those calibrated for events belonging to the 2008/2009 and 2011/2012 periods. This is mainly due to the fact that several waterways have been canalised since 2014 (Ain Smen, Oued El Mehraz, Ain Chkef). It should, however, be noted that the Fez wastewater treatment plant was built in 2014 and, until its construction, the combined sewer outflows as well as the stormwater outflows poured directly into the river. Since 2017, the situation has changed and the higher velocity values may be due to these changes.

Despite measures taken to overcome the risk of overparameterisation, the latter may partly explain the relatively lower performance of the Reservoir3-LR model as compared to SCS-LR, as the number of calibrated parameters for the first model was 5 against 4 for the second one. The use of more calibrated parameters may increase the hydrological modelling uncertainty (Her et al., 2019) and explain the drop in performance during the validation phase (Arsenault et al., 2018). Unfortunately, we did not have access to additional discharge data to calibrate the models spatially and, given the layout of the river network, i.e. unstable cross-sections, canalised inaccessible underground reaches, and the high exposure of the material to theft in some sectors, we could not implement additional intermediate gauging stations.

This study showed that the tested models' performance was higher when rainfall information is provided from multiple rain gauges, which suggests that an additional knowledge of spatial rainfall variability has the potential to improve the models' performance. Pechlivanidis et al. (2009) reached similar conclusions and noted that the reproduction of flood events could be affected if the spatial variability of rainfall is not well represented. Arnaud et al. (2002) also reported similar results in Mexico City, as did Emmanuel et al. (2015) on the Gardon d'Anduze catchment (Southern France) or Ochoa-Rodriguez et al. (2015) on catchments located in Belgium, France, the Netherlands and the UK. Albeit using urban drainage models, Gires et al. (2012) and Bruni et al. (2015) also highlighted the sensitivity of the model outputs to the spatial variability of rainfall. The optimal coverage needed for the Oued Fez catchment is an open question, as implementing rain gauges in the western part of the catchment is not feasible at present due to the

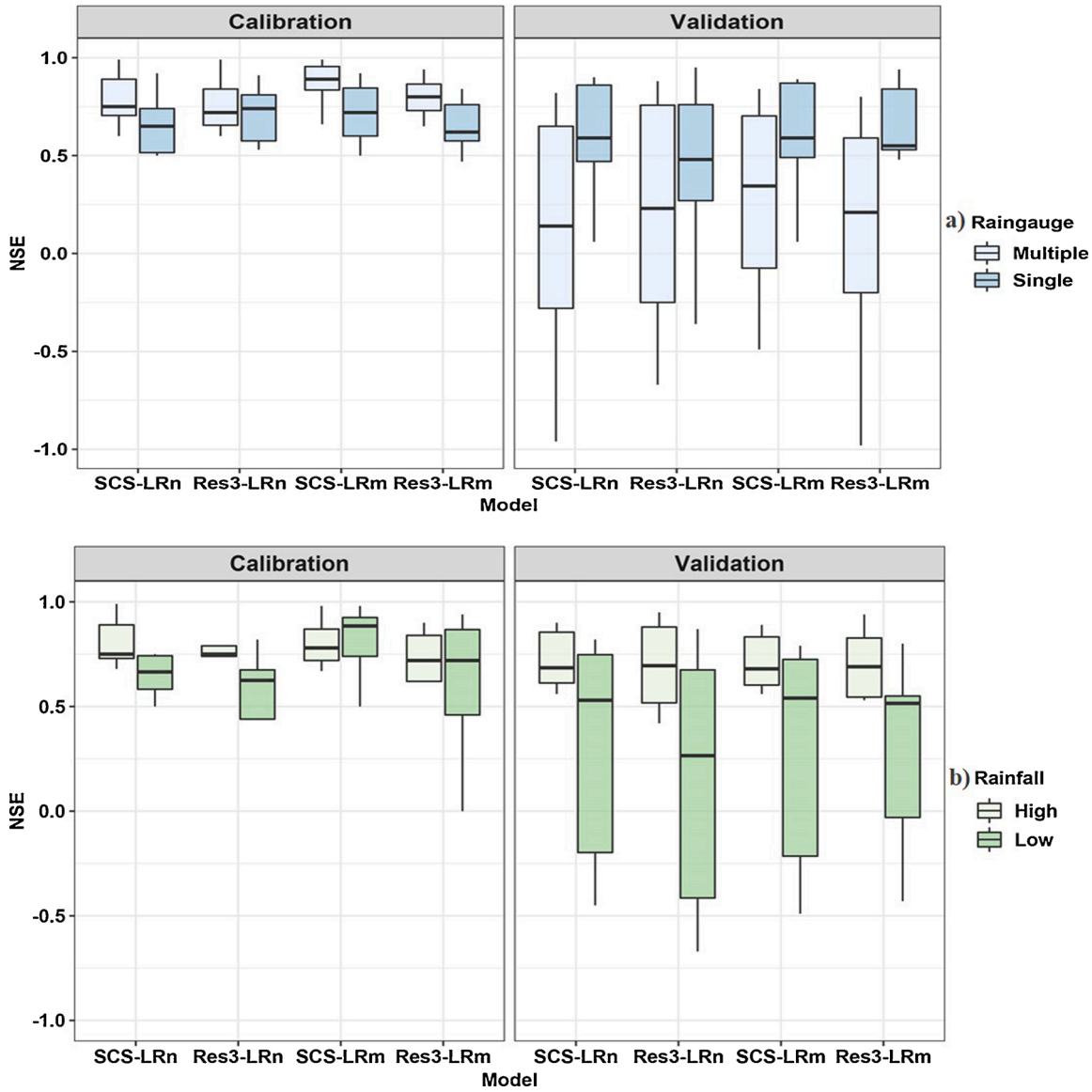

Fig. 12. Comparison of model performance according to a) rainfall depth and b) rain gauge density.

presence of sensitive installations.

Considering the results of the calibration and validation phases at either hourly or 5-minute time steps, it is clear that using the modified drainage network, i.e. forcing drainage directions along the road network and using production classes according to the urbanisation level, ensures better performance than when using the natural drainage network. Additionally, SCS-LR seems to perform better than Reservoir3-LR. This is true in calibration and validation and at both time steps. Thus, even a minimal representation of the urban nature of the catchment, through modified drainage directions and production classes based on the degree of urbanisation, seems to yield better results. This solution was implemented because we did not have access to a map of the stormwater network, and the approach proved to be effective and well adapted to the complex configuration of the Oued Fez catchment. It might be useful elsewhere as well. However, when working on water quality, a separate representation of the stormwater and wastewater networks might be necessary, as flow and in-situ environmental conditions induce bio-chemical transformations that impact solute and particular pollutant fluxes (Chebbo and Gromaire, 2004; Andrés-Doménech et al., 2018). In some West African cities, e.g. Bamako and Ouagadougou, where open-air channels are used for stormwater, field surveys may be carried out to get their geometrical and hydraulic characteristics. In cities like Fez, where the vast majority of these networks are underground, alternative solutions relying on geophysical methods and probabilistic methods may be needed (Bilal et al., 2018).

Using the simple formulation of the lag and route model without interactive cells also has its limitations. The first is that using independent cells would not allow the calculation of discharge values at sub-catchment or street level. This would make the use of such

models limited in urban flooding and inundation studies. However, it is also true that using a simple formulation that relies only on distance makes the transfer function less sensitive to errors on slope values, a common problem in flat environments.

In this application, we used a fully gridded model. If the model's structure had been based on hydrological units and river network segments such as in SWAT (Arnold and Fohrer, 2005) or ModSpa (Moussa et al., 2007), the drainage network's layout would have varied based on the upstream drained area threshold. In our configuration, the network is already "dense" since all the cells are taken into account when calculating the discharge. An alternative would have been to use higher resolution maps where the river network is more densely represented to correct the drainage directions, but such maps were not available for Oued Fez. In addition, many portions of the catchment are "urban stream deserts" (Napieralski et al., 2015), i.e., areas where surface stream channels are not visible because they have been buried or covered by urban development and as such would likely not be reported on maps. This is a major concern for urban catchments as it contributes to the difficulty in defining the hydrographic network.

5. Conclusion

This study has presented an attempt at drainage network representation for distributed hydrological modelling on urban catchments where the layout of the stormwater network is not available. A case study is presented on the Oued Fez catchment using two hydrological models of the ATHYS platform in event-based mode at hourly and 5-minute time steps. Original discharge data recorded at one streamflow gauge and rainfall data recorded at 1–4 rain gauges, depending on the study period, are used to calibrate and validate the selected models. Our findings show that the approach adopted to take into account the urban configuration of the Oued Fez catchment by modifying the drainage directions and by differentiating runoff production according to urbanisation improves the performance of the hydrological models. In addition, comparison of the models in terms of performance shows that the SCS-LR model reproduces the flood hydrographs better than the Reservoir3-LR model regardless of the drainage network and the time step used, although a slight degradation of the models' performance is noted for the sub-hourly time step.

Our results show that when a map of the stormwater network is not available, modellers might use the road network as a proxy to simulate flow at the catchment outlet. However, for water quality studies, this approach might be too limited as in-situ transformations would not be accounted for and contaminant flux calculations would be impacted. Thus, an accurate representation of the stormwater and wastewater networks is still necessary.

By using a fully gridded model where all the cells are used for flow routing, the river network's layout does not vary based on the upstream drained area threshold and thus the modelling results are not impacted by this feature. However, they are prone to uncertainties related to the difficulty in delineating the hydrographic network of urban catchments, which are sometimes buried or covered by urban development.

In addition, using the simple formulation of the lag and route model without interactive cells does not allow discharge calculations at sub-catchment or street level. This would make the use of such models too limited for urban flooding and inundation studies. However, since a simple formulation relies only on the distance to the outlet, it is less sensitive to errors in slope values, a common problem in flat environments. Nevertheless, additional discharge data would be necessary to calibrate the models spatially and to identify the hydrological processes that may need to be accounted for in more specific conceptual models.

Funding

This work was supported by the FP7 EU (Grant number FP7-ENV-2007-1-211732), by the UNF-GPSDD (project "SMART", 2017–2018) and by the French Research Institute for Sustainable Development (IRD).

CRediT authorship contribution statement

Ismail Bouizrou: Writing - original draft, Formal analysis, Software, Visualization. **Nanée Chahinian:** Conceptualization, Methodology, Writing - review & editing, Supervision. **Jean-Louis Perrin:** Methodology, Funding acquisition. **Rémi Müller:** Investigation. **Naoual Rais:** Supervision, Project administration.

Declaration of Competing Interest

The authors report no declarations of interest.

Acknowledgements

The authors would like to acknowledge the Sebou River Basin Authority (Agence du Bassin Hydraulique du Sebou) and the Autonomous Water and Electricity Authority of Fez (Régie Autonome d'Eau et d'Electricité de Fès) for their logistical support.

Appendix A. Supplementary data

Supplementary material related to this article can be found, in the online version, at doi:https://doi.org/10.1016/j.ejrh.2021.100800.

References

ABHS-Agence Hydraulique du Bassin du Sebou, 2005. Etude d'actualisation du plan directeur d'aménagement intégré des ressources en eau du bassin hydraulique du Sebou (PDAIRE). Mission I: Evaluation des ressources en eau du bassin du Sebou. Mission.2: Ressources en eaux souterraines, 106p.

Addor, N., Nearing, G., Prieto, C., Newman, A., Le Vine, N., Clark, M., 2018. A ranking of hydrological signatures based on their predictability in space. Water Resour. Res. 54 (11), 8792–8812.

Akdim, B., Gartet, A., Laaouane, M., Amyay, M., 2013. Flood risk and mitigation strategies in the southeastern suburbs of Fez City (Morocco). Estudios Geográficos LXXIV (275), 379–408.

Ali, M., Onuma, T., Hamada, H., 2012. Quality assessment of digital elevation model derived from ALOS PALSAR interferometry. Remote Sensing 2012, ed. European Association of Geoscientists and Engineers, Paris. https://doi.org/10.3997/2214-4609.20143279.

Aliyari, F., Bailey, R.T., Tasdighi, A., Dozier, A., Arabi, M., Zeiler, K., 2019. Coupled SWAT-MODFLOW model for large-scale mixed agro-urban river basins. Environ. Model. Softw. 115, 200–210. https://doi.org/10.1016/j.envsoft.2019.02.014.

Amarti Riffi, S., 2013. Gerer le reseau d'assainissement de la ville de Fès – Collecter, traiter, valoriser. HTE n° 155. March 2013.

Amiri, M.A., Mesgari, M.S., 2017. Modeling the spatial and temporal variability of precipitation in Northwest Iran. Atmosphere 8 (254), 1–14.

Andréassian, V., Le Moine, N., Perrin, C., Ramos, M.H., Oudin, L., 2012. All that glitters is not gold: the case of calibrating hydrological models. Hydrol. Process. 26, 2206–2210.

Andrés-Doménech, I., Hernández-Crespo, C., Martín, M., Andrés-Valeri, V.C., 2018. Characterization of wash-off from urban impervious surfaces and SuDS design criteria for source control under semi-arid conditions. Sci. Total Environ. 612, 1320–1328. https://doi.org/10.1016/j.scitotenv.2017.09.011.

Arnaud, P., Bouvier, C., Cisneros, L., Dominguez, R., 2002. Influence of rainfall spatial variability on flood prediction. J. Hydrol. 260, 216–230. https://doi.org/10.1016/S0022-1694(01)00611-4.

Arnold, J.G., Fohrer, N., 2005. SWAT2000: current capabilities and research opportunities in applied watershed modeling. Hydrol. Process. 19 (3), 563–572.

Arsenault, R., Brissette, F., Martel, J.L., 2018. The hazards of split-sample validation in hydrological model calibration. J. Hydrol. 566, 346–362. https://doi.org/10.1016/j.jhydrol.2018.09.027.

Bach, P.M., Rauch, W., Mikkelsen, P.S., McCarthy, D.T., Deletic, A., 2014. Environmental modelling & software. A critical review of integrated urban water modelling - Urban drainage and beyond. Environ. Model. Softw. 54, 88–107.

Bannister, E.N., 1979. Impact of road networks on southeastern Michigan lakeshore drainage. Water Resour. Res. 15, 1515–1520. https://doi.org/10.1029/WR015i006p01515.

Barco, J., Wong, K., Stenstrom, M., 2008. Automatic calibration of the U.S. EPA SWMM model for a large urban catchment. Journal of Hydraulic Engineering-ASCE 134. https://doi.org/10.1061/(ASCE)0733-9429(2008)134:4(466).

Bellarbi, M., Rais, N., Mouaddine, A., Elsass, F., Duplay, J., 2011. Physical and chemical characterization of soils from Fez west. 21st International Symposium of Sedimentary Basins. Fez, Morocco.

Beven, K.J., Kirkby, M.J., 1979. A physically based, variable contributing area model of basin hydrology. Hydrol. Sci. Bull. 24 (1), 43–69.

Bilal, M., Khan, W., Muggleton, J., Rustighi, E., Jenks, H., Pennock, S.R., Cohn, A., 2018. Inferring the most probable maps of underground utilities using Bayesian mapping model. J. Appl. Geophy. 150, 52–66. https://doi.org/10.1016/j.jappgeo.2018.01.006.

Bouvier, C., Delclaux, F., 1996. ATHYS: a hydrological environment for spatial modelling and coupling with a GIS. Proc. HydroGIS' 96, Vienna-Austria, IAHS Publication n° 235 19–28.

Bouvier, C., Chahinian, N., Adamovic, M., Cassé, C., Crespy, A., Crès, A., Alcoba, M., 2018. Large scale GIS-based urban flood modelling: a case study on the City of Ouagadougou. In: Gourbesville, P., Cunge, J., Caignaert, G. (Eds.), Advances in Hydroinformatics. Springer, Singapore, pp. 703–717.

Bruni, G., Reinoso, R., Van De Giesen, N.C., Clemens, F.H.L.R., Ten Veldhuis, J.A.E., 2015. On the sensitivity of urban hydrodynamic modelling to rainfall spatial and temporal resolution. Hydrol. Earth Syst. Sci. 19, 691–709. https://doi.org/10.5194/hess-19-691-2015.

Burns, D., Vitvar, T., McDonnell, J., Hassett, J., Duncan, J., Kendall, C., 2005. Effects of suburban development on runoff generation in the Croton River basin, New York, USA. J. Hydrol. 311 (1–4), 266–281.

Chahinian, N., Moussa, R., Andrieux, P., Voltz, M., 2005. Comparison of infiltration models to simulate flood events at the field scale. J. Hydrol. 306, 191–214.

Chahinian, N., Delenne, C., Commandré, B., Derras, M., Deruelle, L., Bailly, J., 2019. Automatic mapping of urban wastewater networks based on manhole cover locations. Comput. Environ. Urban Syst. 78, 101370 https://doi.org/10.1016/j.compenvurbsys.2019.101370.

Chebbo, G., Gromaire, M.C., 2004. The experimental urban catchment "Le Marais" in Paris: what lessons can be learned from it? J. Hydrol. 299 (3–4), 312–323. https://doi.org/10.1016/S0022-1694(04)00372-5.

Chen, W., Huang, G., Zhang, H., Wang, W., 2018. Urban inundation response to rainstorm patterns with a coupled hydrodynamic model: A case study in Haidian Island, China. J. Hydrol. 564, 1022–1035. https://doi.org/10.1016/j.jhydrol.2018.07.069.

Courty, L.G., Soriano-Monzalvo, J.C., Pedrozo-Acuña, A., 2019. Evaluation of open-access global digital elevation models (AW3D30, SRTM, and ASTER) for flood modelling purposes. J. Flood Risk Manag. 12 (Suppl. 1), e12550 https://doi.org/10.1111/jfr3.12550.

Coustau, M., Bouvier, C., Borrell-Estupina, V., Jourde, H., 2012. Flood modelling with a distributed event-based parsimonious rainfall-runoff model: case of the karstic Lez river catchment. Nat. Hazards Earth Syst. Sci. 12, 1119–1133. https://doi.org/10.5194/nhess-12-1119-2012.

Cristiano, E., Ten Veldhuis, M.C., Gaitan, S., Ochoa Rodriguez, S., van de Giesen, N., 2018. Critical scales to explain urban hydrological response: an application in Cranbrook, London. Hydrol. Earth Syst. Sci. 22, 2425–2447. https://doi.org/10.5194/hess-22-2425-2018.

De Luis, M., Gonzalez-Hidalgo, J.C., Brunetti, M., Longares, L.A., 2011. Precipitation concentration changes in Spain 1946–2005. Nat. Hazards Earth Syst. Sci. 11, 1259–1265.

Du, J., Qian, L., Rui, H., Zuo, T., Zheng, D., Xu, Y., Xu, C.-Y., 2012. Assessing the effects of urbanization on annual runoff and flood events using an integrated hydrological modeling system for Qinhuai River basin. China. J. Hydrol. 464–465, 127–139.

Eckhardt, K., 2008. A comparison of baseflow indices, which were calculated with seven different baseflow separation methods. J. Hydrol. 352 (1–2), 168–173. https://doi.org/10.1016/j.jhydrol.2008.01.005.

Emmanuel, I., Andrieu, H., Leblois, E., Janey, N., Payrastre, O., 2015. Influence of rainfall spatial variability on rainfall-runoff modelling: Benefit of a simulation approach? J. Hydrol. 531, 337–348. https://doi.org/10.1016/j.jhydrol.2015.04.058.

Fatichi, S., Vivoni, E., Ogden, F.L., Ivanov, V.Y., Mirus, B., Gochis, D., Tarboton, D., 2016. An overview of current applications, challenges, and future trends in distributed process-based models in hydrology. J. Hydrol. 537, 45–60. https://doi.org/10.1016/j.jhydrol.2016.03.026.

Fewtrell, T., Bates, P., Horritt, M., Hunter, N., 2008. Evaluating the effect of scale in flood inundation modelling in urban environments. Hydrol. Process. 22, 5107–5118. https://doi.org/10.1002/hyp.

Ficchi, A., Perrin, C., Andréassian, V., 2016. Impact of temporal resolution of inputs on hydrological model performance: an analysis based on 2400 flood events. J. Hydrol. 538, 454–470.

Fleischmann, A., Siqueira, V., Paris, A., Collischonn, W., Paiva, R., Pontes, P., Crétaux, J.F., Bergé-Nguyen, M., Biancamaria, S., Gosset, M., Calmant, S., Tanimoun, B., 2018. Modelling hydrologic and hydrodynamic processes in basins with large semi-arid wetlands. J. Hydrol. 561, 943–959. https://doi.org/10.1016/j.jhydrol.2018.04.041.

Fletcher, T.D., Andrieu, H., Hamel, P., 2013. Understanding, management and modelling of urban hydrology and its consequences for receiving waters: a state of the art. Adv. Water Resour. 51, 261–279. https://doi.org/10.1016/j.advwatres.2012.09.001.

Franchini, M., Wendling, J., Obled, C., Todini, E., 1996. Physical interpretation and sensitivity analysis of the TOPMODEL. J. Hydrol. 175, 293–338.

Gaume, E., Livet, M., Desbordes, M., Villeneuve, J., 2004. Hydrological analysis of the river Aude, France, flash flood on 12 and 13 November 1999. J. Hydrol. 286, 135–154.

Gires, A., Onof, C., Maksimovic, C., Schertzer, D., Tchiguirinskaia, I., Simoes, N., 2012. Quantifying the impact of small scale unmeasured rainfall variability on urban runoff through multifractal downscaling: a case study. J. Hydrol. 442–443, 117–128. https://doi.org/10.1016/j.jhydrol.2012.04.005.

Gironas, J., Niemann, J.D., Roesner, L.A., Rodriguez, F., Andrieu, H., 2010. Evaluation of methods for representing urban terrain in storm-water modelling. J. Hydrol. Eng. 15 (1), 1–14.
Graf, W.L., 1977. Network characteristics in suburbanizing streams. Water Resour. Res. 13 (2), 459–463. https://doi.org/10.1029/WR013i002p00459.
Guan, M., Sillanpää, N., Koivusalo, H., 2016. Storm runoff response to rainfall pattern, magnitude and urbanization in a developing urban catchment. Hydrol. Process. 30 (4), 543–557. https://doi.org/10.1002/hyp.10624.
Güneralp, B., Güneralp, İ., Liu, Y., 2015. Changing global patterns of urban exposure to flood and drought hazards. Glob. Environ. Chang. 31, 217–225. https://doi.org/10.1016/j.gloenvcha.2015.01.002.
Guo, X., Fu, D., Wang, J., 2006. Mesoscale convective precipitation system modified by urbanization in Beijing City. Atmos. Res. 82, 112–126. https://doi.org/10.1016/j.atmosres.2005.12.007.
Habibi, H., Seo, D.J., 2018. Simple and modular integrated modeling of storm drain network with gridded distributed hydrologic model via grid-rendering of storm drains for large urban areas. J. Hydrol. 567, 637–653.
Hamed, K., 2008. Trend detection in hydrologic data: the Mann–kendall trend test under the scaling hypothesis. J. Hydrol. 349 (3–4), 350–363. https://doi.org/10.1016/j.jhydrol.2007.11.009.
Hamouda, B., Lahbassi, O., 2012. Integration of pervious area stream flow in urban hydrological model. Energy Procedia 18, 1573–1582.
Haut-Commissariat au Plan, 2020. Le Maroc en chiffres. Accessed on 05/08/2020. https://www.hcp.ma/downloads/Maroc-en-chiffres_t13053.html.
Her, Y., Yoo, S.-H., Cho, J., Hwang, S., Jeong, J., Seong, C., 2019. Uncertainty in hydrological analysis of climate change: multi-parameter vs. multi-GCM ensemble predictions. Sci. Rep. 9 (1), 4974. https://doi.org/10.1038/s41598-019-41334-7.
Huang, H., Cheng, S., Wen, J., Lee, J.-H., 2008. Effect of growing watershed imperviousness on hydrograph parameters and peak discharge. Hydrol. Process. 22, 2075–2085.
Huber, W.C., Dickinson, R.E., 1988. Storm Water Management Model, Version4: User's Manual, EPA600/3-88/001a. Environmental Research Laboratory, EPA, Athens, Georgia.
Hughes, D.A., 1994. Soil moisture and runoff simulations using four catchment rainfall-runoff models. J. Hydrol. 158, 381–404.
INSAVALOR, SOGREAH, 1997. CANOE- Logiciel d'hydrologie urbaine. Conception et évaluation de réseaux d'assainissement. Simulation des pluies, des écoulements et de la qualité des eaux. Manuel de l'utilisateur.
Jain, S.K., Kumar, V., 2012. Trend analysis of rainfall and temperature data for India. Curr. Sci. 102, 37–49.
Jakeman, A.J., Hornberger, G.M., 1993. How much complexity is warranted in a rainfall-runoff model? Water Resour. Res. 29, 2637–2649.
Jankowfsky, S., Branger, F., Braud, I., Rodriguez, F., Debionne, S., Viallet, P., 2014. Assessing anthropogenic influence on the hydrology of small peri-urban catchments: development of the object-oriented PUMMA model by integrating urban and rural hydrological models. J. Hydrol. 517, 1056–1071. https://doi.org/10.1016/j.jhydrol.2014.06.034.
Kendall, M.G., 1975. Rank Correlation Methods, 4th ed. Charles Griffin, London.
Kisi, O., 2015. An innovative method for trend analysis of monthly pan evaporations. J. Hydrol. 527, 1123–1129.
Klemeš, V., 1986. Operational testing of hydrological simulation models. Hydrological Sciences 3 (1–3), 13–24.
Koukkal, B., Dominik, J., Vignati, D., Arpagaus, P., Santiago, S., Ouddane, B., Benaabidate, L., 2004. Assessment of water quality and toxicity of polluted rivers Fez and Sebou in the region of Fez (Morocco). Environ. Pollut. 131 (163–1), 72.
Krebs, G., Kokkonen, T., Valtanen, M., Setälä, H., Koivusalo, H., 2014. Spatial resolution considerations for urban hydrological modelling. J. Hydrol. 512, 482–497. https://doi.org/10.1016/j.jhydrol.2014.03.013.
Kroczak, R., Bryndal, T., 2015. An attempt to assess the influence of road network on flash flood wave parameters. The case study of the Carpathian foothills. In: Jasiewicz, Z., Zwoliński, Z., Mitasova, H., Hengl, T. (Eds.), Geomorphometry for Geosciences. Adam Mickiewicz University in Poznań - Institute of Geoecology and Geoinformation. International Society for Geomorphometry, Poznań, pp. 197–200.
Laganier, O., Ayral, P.A., Salze, D., Sauvagnargues, S., 2014. A coupling of hydrologic and hydraulic models appropriate for the fast floods of the Gardon River basin (France). Nat. Hazards Earth Syst. Sci. 14, 2899–2920. https://doi.org/10.5194/nhess-14-2899-2014.
Le Coz, J., Chaléon, C., Bonnifait, L., Le Boursicaud, R., Renard, B., Branger, F., Valente, M., 2013. Analyse bayésienne des courbes de tarage et de leurs incertitudes: la méthode BaRatin. Houille Blanche (6), 31–41. https://doi.org/10.1051/lhb/2013048.
Leandro, J., Martins, R., 2016. A methodology for linking 2D overland flow models with the sewer network model SWMM 5.1 based on dynamic link libraries. Water Sci. Technol. 73 (12), 3017–3026.
Leandro, J., Schumann, A., Pfister, A., 2016. A step towards considering the spatial heterogeneity of urban key features in urban hydrology flood modelling. J. Hydrol. 535, 356–365. https://doi.org/10.1016/j.jhydrol.2016.01.060.
Lhomme, J., Bouvier, C., Perrin, J.L., 2004. Applying a GIS-based geomorphological routing model in urban catchments. J. Hydrol. 299, 203–216.
Lhomme, J., Bouvier, C., Mignot, E., Paquier, A., 2006. One-dimensional GIS-based model compared with a two-dimensional model in urban floods simulation. Water Sci. Technol. 54, 83–91. https://doi.org/10.2166/wst.2006.594.
Li, C., Liu, M., Hu, Y., Shi, T., Qu, X., Walter, M.T., 2018. Effects of urbanization on direct runoff characteristics in urban functional zones. Sci. Total Environ. 643, 301–311. https://doi.org/10.1016/j.scitotenv.2018.06.211.
Liang, P., Ding, Y., 2017. The long-term variation of extreme heavy precipitation and its link to urbanization effects in Shanghai during 1916–2014. Adv. Atmos. Sci. 34, 321–334. https://doi.org/10.1007/s00376-016-6120-0.
Lombard-Latune, R., Chahinian, N., Perrin, J.L., Benaabidate, L., Lahrach, A., 2010. Hydrological processes controlling flow generation in a Mediterranean urbanized catchment. In: Proceedings of the 6th World FRIEND Conference, 25–29 October, 2010. Global Change: Facing Risks and Threats to Water Resources, IAHS Publication 340, pp. 69–76.
Maier, R., Krebs, G., Pichler, M., Muschalla, D., Gruber, G., 2020. Spatial rainfall variability in urban environments - high-density precipitation measurements on a city-scale. Water (Switzerland) 12 (4), 1157. https://doi.org/10.3390/W12041157.
Mann, H.B., 1945. Nonparametric tests against trend. Econometrica 13, 245–259.
MATNUHPV-Ministère de l'Aménagement du Territoire National, de l'Urbanisme, de l'Habitat et de la Politique de la Ville, 2019. Etude d'élaboration du schéma directeur d'aménagement urbain du grand Fès. PHASE 2: Options et choix d'aménagement, 254p.
McMillan, H., Seibert, J., Petersen-Overleir, A., Lang, M., White, P., Snelder, T., et al., 2017. How uncertainty analysis of streamflow data can reduce costs and promote robust decisions in water management applications. Water Resour. Res. 53, 5220–5228. https://doi.org/10.1002/2016WR020328.
METLE-Ministère de l'Équipement, du Transport, de la Logistique et de l'Eau. 2020. http://81.192.10.228/patrimoine/barrages/barrages-existants/#1454512985304-fbbef6f4-8bbc.
Meyer, J.L., Wallace, J.B., 2001. Lost linkages and lotic ecology: rediscovering small streams. In: Press, M.C., Huntly, N.J., Levin, S. (Eds.), Ecology, Achievement and Challenge. Blackwell Science, Malden, Massachusetts, pp. 295–317.
Michaud, J., Sorooshian, S., 1994. Comparison of simple versus complex distributed runoff models on a midsized semiarid watershed. Water Resour. Res. 30 (3), 593–605. https://doi.org/10.1029/93WR03218.
Miller, J., Kim, K., Kjeldsen, R., Packman, J., Grebby, S., Dearden, D., 2014. Assessing the impact of urbanization on storm runoff in a peri-urban catchment using historical change in impervious cover. J. Hydrol. 515, 67–69.
Moussa, R., Chahinian, N., Bocquillon, C., 2007. Distributed hydrological modelling of a Mediterranean mountainous catchment - Model construction and multi-site validation. J. Hydrol. 337 (1–2), 35–51. https://doi.org/10.1016/j.jhydrol.2007.01.028.
MUAT-Ministère de l'Urbanisme et de l'Aménagement du Territoire, 2016. Etude d'élaboration du schéma directeur d'aménagement urbain du grand Fès. Phase 1: diagnostic territorial et enjeux de développement. Rapport de synthèse, 77p.
Napieralski, J., Keeling, R., Dziekan, M., Rhodes, C., Kelly, A., Kobberstad, K., 2015. Urban stream deserts as a consequence of excess stream burial in urban watersheds. Ann. Assoc. Am. Geogr. 105 (4), 649–664. https://doi.org/10.1080/00045608.2015.1050753.

Nash, J.E., Sutcliffe, J.V., 1970. River flow forecasting through conceptual models: part I-A: discussion of principles. J. Hydrol. 10 (3), 282–290. https://doi.org/10.1016/0022-1694(70)90255-6.
Ngula Niipele, J., Chen, J., 2019. The usefulness of ALOS-PALSAR DEM data for drainage extraction in semi-arid environments in the Iishana sub-basin. J. Hydrol. Reg. Stud. 21, 57–67. https://doi.org/10.1016/j.ejrh.2018.11.003.
Nguyen, S., Bouvier, C., 2019. Flood modelling using the distributed event-based SCS-LR model in the Mediterranean Real Collobrier catchment. Hydrol. Sci. J. Des Sci. Hydrol. 64, 1351–1369. https://doi.org/10.1080/02626667.2019.1639715.
O'Callaghan, J., Mark, D., 1984. The extraction of drainage networks from digital elevation data. Comput. Vis. Graph. Image Process. 28, 323–344. https://doi.org/10.1016/0734-189X(89)90053-4.
Ochoa-Rodriguez, S., Wang, L.P., Gires, A., Pina, R.D., Reinoso-Rondinel, R., Bruni, G., Ichiba, A., Gaitan, S., Cristiano, E., Van Assel, J., Kroll, S., Murlà-Tuyls, D., Tisserand, B., Schertzer, D., Tchiguirinskaia, I., Onof, C., Willems, P., Ten Veldhuis, M.C., 2015. Impact of spatial and temporal resolution of rainfall inputs on urban hydrodynamic modelling outputs: a multi-catchment investigation. J. Hydrol. 531, 389–407. https://doi.org/10.1016/j.jhydrol.2015.05.035.
Ogden, F.L., Raj Pradhan, N., Downer, C.W., Zahner, J.A., 2011. Relative importance of impervious area, drainage density, width function, and subsurface storm drainage on flood runoff from an urbanized catchment. Water Resour. Res. 47 (12), 1–12. https://doi.org/10.1029/2011WR010550.
Oliver, J.E., 1980. Monthly precipitation distribution: a comparative index. Prof. Geogr. 32 (3), 300–309.
Palla, A., Gnecco, I., 2015. Hydrologic modeling of low impact development systems at the urban catchment scale. J. Hydrol. 528, 361–368. https://doi.org/10.1016/j.jhydrol.2015.06.050.
Paquier, A., Mignot, E., Bazin, P.H., 2015. From hydraulic modelling to urban flood risk. Procedia Eng. 115 (i), 37–44. https://doi.org/10.1016/j.proeng.2015.07.352.
Pechlivanidis, I.G., McIntyre, N., Wheater, H., 2009. The significance of spatial rainfall on runoff generation. In: Proceedings of the iEMSs Fourth Biennial Meeting: International Congress on Environmental Modelling and Software (iEMSs 2008), International Environmental Modelling and Software Society (iEMSs), 2008. Barcelona, pp. 478–485.
Pérez-Sánchez, J., Senent-Aparicio, J., Segura-Méndez, F., Pulido-Velazquez, D., Srinivasan, R., 2019. Evaluating hydrological models for deriving water resources in Peninsular Spain. Sustainability 11 (10), 2872. https://doi.org/10.3390/su11102872.
Perrin, J.L., Bouvier, C., 2004. Rainfall-runoff modelling in the urban catchment of El Batan, Quito, Ecuador. Urban Water J. 1 (4), 299–308.
Perrin, J.L., Raïs, N., Chahinian, N., Moulin, P., Ijjaali, M., 2014. Water quality assessment of highly polluted rivers in a semi-arid Mediterranean zone Oued Fez and Sebou River (Morocco). J. Hydrol. 510, 26–34. https://doi.org/10.1016/j.jhydrol.2013.12.002.
Refsgaard, J.C., Storm, B., 1995. MIKE SHE. In: Singh, V.P. (Ed.), Computer Models of Watershed Hydrology. Water Resource Publications, CO, USA, pp. 806–846.
Reynard, E., Werren, G., Lasri, M., Obda, K., El Khalki, Y., 2013. Cartes des phénomènes d'inondation de deux bassins versants marocains: problèmes méthodologiques. Mémoire Société Vaudoise des Sciences Naturelles 25, 71–81.
Rodriguez, F., Andrieu, H., Zech, Y., 2000. Evaluation of a distributed model for urban catchments using a 7-year continuous data series. Hydrol. Process. 14, 899–914.
Rodriguez, F., Andrieu, H., Creutin, J.D., 2003. Surface runoff in urban catchments: morphological identification of unit hydrographs from urban databanks. J. Hydrol. 283 (1–4), 146–168. https://doi.org/10.1016/S0022-1694(03)00246-4.
Rodriguez, F., Andrieu, H., Morena, F., 2008. A distributed hydrological model for urbanized areas – model development and application to case studies. J. Hydrol. 351 (3–4), 268–287.
Salvadore, E., Bronders, J., Batelaan, O., 2015. Hydrological modelling of urbanized catchments: a review and future directions. J. Hydrol. 529, 62–81.
Samadi, A., Sadrolashrafi, S., Kholghi, M., 2019. Development and testing of a rainfall-runoff model for flood simulation in dry mountain catchments: a case study for the Dez River Basin. Phys. Chem. Earth 109, 9–25. https://doi.org/10.1016/j.pce.2018.07.003.
Schmitt, T.G., Thomas, M., Ettrich, N., 2004. Analysis and modeling of flooding in urban drainage systems. J. Hydrol. 299 (3–4), 300–311. https://doi.org/10.1016/S0022-1694(04)00374-9.
Segond, M., Wheater, H., Onof, C., 2007. The significance of spatial rainfall representation for flood runoff estimation: A numerical evaluation based on the Lee catchment, UK. J. Hydrol. 347, 116–131.
Sen, P.K., 1968. Estimates of the regression coefficient based on Kendall's tau. J. Am. Stat. Assoc. 63, 1379–1389.
Shimadera, H., Kondo, A., Shrestha, K.L., Kitaoka, K., Inoue, Y., 2015. Numerical evaluation of the impact of urbanization on summertime precipitation in Osaka, Japan. Adv. Meteorol. https://doi.org/10.1155/2015/379361.
Shuster, W.D., Bonta, J., Thurston, H., Warnemuende, E., Smith, D.R., 2005. Impacts of impervious surface on watershed hydrology: a review. Urban Water J. 2 (4), 263–275. https://doi.org/10.1080/15730620500386529.
Soil Conservation Service-USDA, 1972. Estimation of direct runoff from storm rainfall. National Engineering Handbook. Section 4-Hydrology, pp. 10.1–10.24.
Steenhuis, S., Winchell, M., Rossing, J., Zollweg, J., Walter, M., 1995. SCS runoff equation revisited for variable-source runoff areas. J. Irrig. Drain. Eng. 121, 234–238.
Stewart, M., 2015. Promising new baseflow separation and recession analysis methods applied to streamflow at Glendhu Catchment, New Zealand. Hydrol. Earth Syst. Sci. 19 (6), 2587–2603. https://doi.org/10.5194/hess-19-2587-2015.
Tabari, H., Talaee, P.H., 2011. Analysis of trends in temperature data in arid and semiarid regions of Iran. Global Planet Change 79, 1–10.
Tarboton, D.G., Bras, R.L., Rodriguez-Iturbe, I., 1991. On the extraction of channel networks from digital elevation data. Hydrol. Process. 5 (1), 81–100. https://doi.org/10.1002/hyp.3360050107.
Tegegne, G., Park, D.K., Kim, Y.O., 2017. Comparison of hydrological models for the assessment of water resources in a data-scarce region, the Upper Blue Nile River Basin. J. Hydrol. Reg. Stud. 14, 49–66.
Tramblay, Y., Bouvier, C., Crespy, A., Marchandise, A., 2010a. Improvement of flash flood modelling using spatial patterns of rainfall: a case study in south of France. In: IAHS Publ.Global Change: Facing Risks and Threats to Water Resources Proceedings of the Sixth World FRIEND Conference, Fez, Morocco, October 2010, 340, pp. 172–178. http://y.tramblay.free.fr/doc/Tramblay-redbook.
Tramblay, Y., Bouvier, C., Martin, C., Didon-Lescot, J.-F., Todorovik, D., Domergue, J.-M., 2010b. Assessment of initial soil moisture conditions for event-based rainfall–runoff modelling. J. Hydrol. 387, 176–187.
Tramblay, Y., Bouvier, C., Ayral, P.-A., Marchandise, A., 2011. Impact of rainfall spatial distribution on rainfall-runoff modeling efficiency and initial soil moisture conditions estimation. Nat. Hazards Earth Syst. Sci. 12. https://doi.org/10.5194/nhess-11-157.
Wang, J., Hu, C., Ma, B., Mu, X., 2020. Rapid urbanization impact on the hydrological processes in Zhengzhou, China. Water (Switzerland) 12 (7). https://doi.org/10.3390/W12071870.
Xu, Z., Zhao, G., 2016. Impact of urbanization on rainfall-runoff processes: case study in the Liangshui River Basin in Beijing, China. Proc. IAHS 373, 9–12.
Yao, L., Wei, W., Chen, L., 2016. How does imperviousness impact the urban 729 rainfall-runoff process under various storm cases? Ecol. Indic. 60, 893–905.
Yue, S., Pilon, P., Phinney, B., Cavadias, G., 2002. The influence of autocorrelation on the ability to detect trend in hydrological series. Hydrol. Process. 16, 1807–1829.
Zambrano, L., Pacheco-Muñoz, R., Fernández, T., 2018. Influence of solid waste and topography on urban floods: the case of Mexico city. Ambio 47 (7), 771–780. https://doi.org/10.1007/s13280-018-1023-1.
Zhang, C.L., Chen, F., Miao, S.G., Li, Q.C., Xuan, C.Y., 2007. Influences of urbanization on precipitation and water resources in the metropolitan Beijing area. In: San Antonio, TX, USA87th AMS Annu. Meet. Proceedings of the 21st American Metrological Society Conference on Hydrology, vol. 17.
Zhu, X., Zhang, Q., Sun, P., Singh, V.P., Shi, P., Song, C., 2019. Impact of urbanization on hourly precipitation in Beijing, China: spatiotemporal patterns and causes. Glob. Planet. Change 172, 307–324. https://doi.org/10.1016/j.gloplacha.2018.10.018.
Zoppou, C., 2000. Review of urban stormwater models. Environ. Model. Softw. 16, 195–231.